

Training neural networks with structured noise improves classification and generalization

Marco Benedetti^{1,*} and Enrico Ventura^{1,2,*}

¹*Dipartimento di Fisica, Sapienza Università di Roma, P.le A. Moro 2, 00185 Roma, Italy*

²*Laboratoire de Physique de l'Ecole Normale Supérieure, ENS, Université PSL, F-75005 Paris, France*

The beneficial role of noise in learning is nowadays a consolidated concept in the field of artificial neural networks, suggesting that even biological systems might take advantage of similar mechanisms to maximize their performance. The training-with-noise algorithm proposed by Gardner and collaborators is an emblematic example of a noise injection procedure in recurrent networks, which are usually employed to model real neural systems. We show how adding structure into noisy training data can substantially improve the algorithm performance, allowing to approach perfect classification and maximal basins of attraction. We also prove that the so-called Hebbian unlearning rule coincides with the training-with-noise algorithm when noise is maximal and data are fixed points of the network dynamics. A sampling scheme for optimal noisy data is eventually proposed and implemented to outperform both the training-with-noise and the Hebbian unlearning procedures.

I. INTRODUCTION

The development of models and tools from theoretical physics has greatly contributed to our understanding of how the brain is able to learn concepts [1]. An initial approach to brain modeling used recurrent networks composed of binary neurons connected through pairwise interactions. Each neuron could be either *active* or *silent* based on the signals received from neighboring neurons. By incorporating realistic rules for updating neuron states (i.e. the neural dynamics), these networks exhibited dynamic multistability, resulting in the formation of many attractors. These systems, called *attractor neural networks*, besides being similar in structure to biological neural networks, resembled well-known models in the physics of disordered systems [2]. The landscape of attractors and their existence depended on both the dynamics and choice of couplings between neurons. The processes of modification of the interactions, necessary to guarantee that concepts presented to the network as external stimuli were stored and retrieved as attractors, is studied in neuroscience under the name of *synaptic plasticity processes*. They are modeled by physicists with discrete time *learning algorithms*, that see a set of *training data* (i.e. the concepts themselves or some representations of them) and update the interactions to reinforce memory retrieval.

Modern artificial neural networks, that make use of deep and non-recurrent architectures, also exploit the same principle to train connections between neurons from a data-set and manage to perform a task (e.g. classification, generation of new data). An important notion in this context is *overfitting*, namely when a model becomes too focused on the details of the specific training set, instead of understanding the broader structure highlighted by the data. In this case one says that *generalization* to unseen samples is lacking in the system. This concept

can be exported to attractor neural networks, where an overfitting model would translate into a system which is not able to associate corrupted versions of a concept to the concept itself. An important challenge for modern artificial neural networks is to improve generalization by means of regularization techniques. One class of techniques relies on injecting noise in the training process, with the idea of teaching the machine how to better infer the hidden data structure from errors. Examples of these types of regularization are the drop-out [3–6] or data-augmentation procedures [7, 8]. The former consists in stochastically deactivating neurons across the network (or even only on the input layer) during training, the latter acts on the training data themselves, by performing transformations (e.g. translations, rotations) to increase the heterogeneity of the data-set. Even if such procedures are practical and successful in the matter of deep networks, there are only few examples of theory-based criteria for choosing how to engineer noise to inject in the training [4, 8].

Our work considers a simple learning algorithm employing noise-injection in the training process, acting on attractor neural networks. We are interested in this type of networks for multiple reasons: they are suitable to be modeled through the tools of statistical mechanics; they show some biological interest, especially in the perspective of introducing unsupervised kinds of learning dynamics. The main objective of our study is to establish a theoretical criterion for generating the most effective noise to be utilized in training, thereby optimizing the performance of an associative memory model. Specifically, we demonstrate that generating optimal noise translates into producing training data-points whose features adhere to specific constraints, which we refer to as the *structure* of the noise. We will also delineate some important connections between training procedures with optimally structured noise and other consolidated learning prescriptions present in literature, such as the Hebbian unlearning rule. Our analysis thus takes place at the interface between three disciplines: statistical physics, artificial intelligence

* The two authors contributed equally

and neuroscience. We are now completing this introductory section by presenting the mathematical model underneath our study and some important learning procedures that will be relevant to the analysis.

A. Attractor neural networks

We consider a fully connected network of N binary variables $\{S_i = \pm 1\}$, $i \in [1, \dots, N]$, linked by couplings J_{ij} . The network is endowed with a dynamics

$$S_i(t+1) = \text{sign} \left(\sum_{j=1}^N J_{ij} S_j(t) \right), \quad i = 1, \dots, N \quad (1)$$

which can be run either in parallel (i.e. *synchronously*) or in series (i.e. *asynchronously* in a random order) over the i indices. We will mainly concentrate on asynchronous dynamics, in which case eq. (1) can only converge to fixed points, when they exist [1]. This kind of network can be used as an associative memory device, namely for reconstructing a number p of configurations $\{\xi_i^\mu\} = \pm 1$, $\mu \in [1, \dots, p]$, called *memories*, when the dynamics is initialized into a configuration similar enough to one of them. In this work, we will concentrate on i.i.d. memories, generated with a probability $P(\xi_i^\mu = \pm 1) = 1/2$. With an appropriate choice of the couplings, the model can store an extensive number of memories $p = \alpha N$, where α is called *load* of the network.

1. Characterizing the performance of an Attractor Neural Network

We now describe how to benchmark the neural network performance, specifically in terms of the dynamic stability achieved by the memory vectors and the ability of the system to retrieve blurry examples of the latter.

We define *classification* as the capability to perfectly retrieve each memory when the dynamics is initialized to the memory itself. The fraction among all pN units ξ_i^μ that are stable according to one step of the dynamics (1) will be called n_{SAT} , in analogy with previous celebrated optimization problems [9, 10]. Classification is reached when $n_{SAT} = 1$. It is here convenient to define a quantity, called *stability*, and defined as it follows

$$\Delta_i^\mu = \frac{\xi_i^\mu}{\sqrt{N\sigma_i}} \sum_{j=1}^N J_{ij} \xi_j^\mu, \quad \sigma_i = \sqrt{\sum_{j=1}^N J_{ij}^2 / N}. \quad (2)$$

It is important to remark the following implication of statements

$$n_{SAT} = 1 \iff \Delta_i^\mu > 0 \ \forall i, \mu \quad (3)$$

We furthermore define *generalization* as the capability to retrieve the memory, or a configuration that is

strongly related to it, by initializing the dynamics on a noise-corrupted version of the memory. This property of the neural network is related to the size of the basins of attraction to which the memories belong, and does not imply $n_{SAT} = 1$. A good measure of the performance in this sense is the *retrieval map*

$$\overline{m_f}(m_0) := \overline{\left\langle \frac{1}{N} \sum_{i=1}^N \xi_i^\nu S_i^\nu(\infty) \right\rangle}. \quad (4)$$

Here, $\vec{S}^\nu(\infty)$ is the stable fixed point reached by the network, when it exists, when the dynamics is initialized to a configuration $\vec{S}^\nu(0)$ having overlap m_0 with a given memory $\vec{\xi}^\nu$. The symbol $\overline{\cdot}$ denotes the average over different realizations of the memories and $\langle \cdot \rangle$ the average over different realizations of $\vec{S}^\nu(0)$. In the classification regime, one obtains $m_f = 1$ when $m_0 = 1$. The analytical computation of the retrieval map might be challenging for some networks, especially for fully connected ones. Hence, one can introduce another indicative observable for the generalization, i.e. the *one-step retrieval map* $m_1(m_0)$ [11], defined by applying a single step of *synchronous* dynamics (1):

$$\overline{m_1}(m_0) := \overline{\left\langle \xi_i^\nu \text{sign} \left(\sum_{j=1}^N J_{ij} S_j^\nu(0) \right) \right\rangle}, \quad (5)$$

This work is devoted to exploring the characteristics of the training process leading to classification and good generalization.

B. Learning algorithms

We now provide for some notable examples of learning rules implemented on recurrent neural networks, which will often be mentioned in the rest of this work. All these procedures can be conceived as an iterative modification of the couplings on the basis of an initial choice of the couplings and a set of training data presented to the network.

1. Hebb's rule

Hebb's (or Hebbian) learning prescription [12, 13] consists in building up the connections between the neurons as an empirical covariance of the memories, i.e.

$$J_{ij}^H = \frac{1}{N} \sum_{\mu=1}^p \xi_i^\mu \xi_j^\mu. \quad (6)$$

This rudimentary yet effective rule allows to retrieve memories up to a critical capacity $\alpha_c^H = 0.138$. [14]. Notably, when $\alpha < \alpha_c^H$ memories are not perfectly recalled, but only reproduced with a small number of errors. On the other hand, when $\alpha > \alpha_c^H$ the statistical interference between the random memories impedes

the dynamics to retrieve them, shifting the system into an oblivion regime. Notably, the landscape of attractors given by this rule is rugged and disseminated with *spurious states*, i.e. stable fixed points of the dynamics barely overlapped with the original memories.

2. Linear Perceptron & Support Vector Machine (SVM)

The linear perceptron algorithm [9, 10, 15], widely recognized as the very basis of modern artificial intelligence, is an iterative procedure allowing to fully stabilize the memories and tune their generalization capabilities. Specifically, we are going to refer to *linear perceptron* as the adaptation of the classical perceptron to recurrent neural networks, already introduced in [9, 15–18]. In this case, a N -dimensional input layer is fully connected by the connections J to a N -dimensional output layer. This architecture can be mapped into a biologically inspired recurrent neural network. Given the fully connected architecture, we want to find a set of couplings that satisfies the constraints

$$\Delta_i^\mu > k, \quad \forall \mu, i, \quad (7)$$

with k being a control parameter called *margin*. Given a value of α , constraint eq. (7) is satisfiable up to a maximum value of $k_{\max}(\alpha)$. The maximum capacity achievable by the network is $\alpha_c^P = 2$, with $k_{\max}(2) = 0$. Inside these limits, all constraints in (7) will be satisfied after a number of iterations of the following serial update for the couplings

$$\begin{aligned} \delta J_{ij}^{(d)} &= \lambda \sum_{\mu=1}^p \epsilon_i^\mu \xi_i^\mu \xi_j^\mu, \quad J_{ii} = 0, \\ \epsilon_i^\mu &= \frac{1}{2} (1 + \text{sign}(k - \Delta_i^\mu)), \end{aligned} \quad (8)$$

where λ is a small positive learning rate and d is the algorithm time step. One can also symmetrize equation (8) by redefining the mask ϵ_i^μ as

$$\epsilon_i^\mu \rightarrow \epsilon_{ij}^\mu = \frac{1}{2} (\epsilon_i^\mu + \epsilon_j^\mu),$$

obtaining a lower critical capacity and a general decreasing of the function $k_{\max}(\alpha)$ due to the imposition of the symmetry [15, 19]. It has been proved numerically that, given α , the larger k is, with $0 < k < k_{\max}(\alpha)$, the wider are the basins of attraction. In line with the past literature [16, 20] we call a maximally stable perceptron, such that $k = k_{\max}(\alpha)$, a Support Vector Machine (SVM).

3. Hebbian unlearning

Inspired by the brain functioning during REM sleep [21], the Hebbian unlearning algorithm (HU) [19, 21–24] is a training procedure leading to classification and good

generalization in a symmetric neural network. Training starts by initializing the connectivity matrix according to Hebb's rule eq. (6) (i.e. $J^0 = J^H$). Then, the following procedure is iterated at each step d :

1. Initialize of the network dynamics (1) on a random neural state.
2. Run the asynchronous dynamics until convergence to a stable fixed point $\vec{S}^{(d)}$.
3. Update couplings according to:

$$\delta J_{ij}^{(d)} = -\frac{\lambda}{N} S_i^{(d)} S_j^{(d)}, \quad J_{ii} = 0 \quad \forall i, \quad \lambda > 0 \quad (9)$$

where λ is a small learning rate. This algorithm was first introduced to prune the landscape of attractors from proliferating spurious states, i.e. fixed points of (1) not coinciding with the memories [1, 25]. Such spurious states are only weakly correlated with the memories. Even though this pruning action leads to the full stabilization of the memories, the exact mechanism behind this effect is not completely understood. The analysis in [19] gives deeper insights in both the classification and generalization capabilities of a network trained with HU. The classification property is achieved running the algorithm when $\alpha \leq \alpha_c^U$ with $\alpha_c^U \simeq 0.6$. To quantify the classification performance of the network, one can track numerically the observable

$$\Delta_{\min} = \overline{\min_{i,\mu} (\Delta_i^\mu)}, \quad (10)$$

where Δ_i^μ are the stabilities of the network and the symbol $\overline{\cdot}$ denotes the average over different realizations of the memories. As soon as $\Delta_{\min} > 0$, memories become fixed points of the dynamics [9].

The left panel on fig. 1 reports the evolution of Δ_{\min} as a function of the number of performed updates of J , for $\alpha = 0.3$. The amount of iterations $d = D_{in}$ (indicated with a red circle) marks when Δ_{\min} crosses 0. At this point, all the memories are fixed points of the dynamics. Other two points, $d = (D_{top}, D_{fin})$ with λ , N and α are reported in the plot, even though [19] has proved D_{in} to show the best generalization performance in the large N limit. The scaling of $(D_{in}, D_{top}, D_{fin})$ is also described in [19]. The progressive decay of Δ_{\min} , that becomes negative again after $d = D_{fin}$, is due to the vanishing of the first two moments of the couplings. HU creates large basins of attraction around the memories, when $\alpha < \alpha_c^U$. The right panel on fig. 1 reports the retrieval map for $N = 100$ and $\alpha = 0.3$. The curves relative to the SVM and unlearning at $d = D_{in}$ coincide. This observation is coherent with estimates for the large N limit performed in [19]. The SVM is trained with no symmetry constraints. Still, its performance does not differ from the symmetric SVM discussed in [15, 19, 26]: this is due to the high degree of symmetry displayed by SVMs, something that partially emerges from the past literature [18] but still deserves further investigations. Fig. 1 also

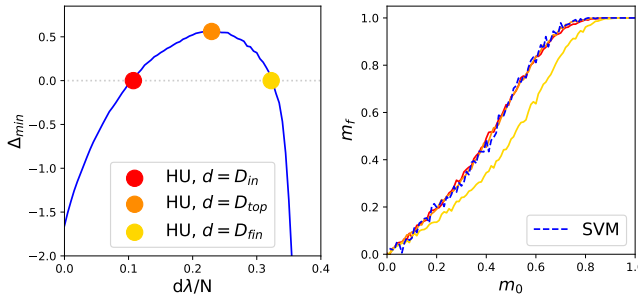


FIG. 1: Left: The minimum stability Δ_{\min} as a function of the normalized algorithm time. The threshold $\Delta = 0$ is indicated with the *gray dotted line*. Three relevant amount of iterations are indicated by the colored circles: $d = D_{in}$ in *red*, $d = D_{top}$ in *orange*, $d = D_{fin}$ in *yellow*. All measures are averaged over 50 realizations of the network. Right: Retrieval map $m_f(m_0)$ for a SVM and the unlearning algorithm at the three relevant steps $\{D_{in}, D_{top}, D_{fin}\}$, with the same color code used on the plot on the left panel. All measures are averaged over 10 realizations of the network. Choice of the parameters: $N = 100$, $\alpha = 0.3$, $\lambda = 10^{-2}$.

shows that curves for $d = D_{in}$ and $d = D_{top}$ overlap significantly. This is certainly due to finite size effects, since [19] clearly shows the basins to progressively shrink, in the large N limit, when d is increased beyond D_{in} . Why the optimum is found when $\Delta_{\min} = 0$ (i.e. $d = D_{in}$) and not when Δ_{\min} is maximum (i.e. $d = D_{top}$) is an open question. A second question regards why HU, and the choice of using fixed points as training data, should lead to maximally large basins of attraction.

C. Outline of the research

We now provide an overview of the key procedures employed in our analysis. To begin, Section II introduces and characterizes the *training-with-noise* algorithm proposed by [27], emphasizing its comparison with the SVMs discussed in the Introduction. In Section III, we mathematically derive the conditions for optimal noisy training data, specifically focusing on the extreme case of injecting maximal noise. The main objective of this study is to demonstrate that substantial improvements can be achieved in the training-with-noise algorithm, when the training data incorporates internal dependencies, referred to as *structure*. Moving on to Section IV, we elucidate how the HU rule emerges from the training-with-noise procedure, particularly when maximum noise is applied and the training data is selected as fixed points of eq. (1). Finally, in Section V, we present the development of an effective sampler device for generating good noisy training data, which enables the achievement of higher critical capacities while preserving sizable basins of attraction for the memories.

II. TRAINING WITH NOISE

The concept of learning from noisy examples, introduced for the first time in [28], is at the basis of a study performed by Gardner and co-workers [27], a pioneering attempt to increase and control generalization through the introduction of noise during the training phase of recurrent neural networks. Here, we report the algorithm and characterize, for the first time, its performance over fully connected neural networks.

The training-with-noise (TWN) algorithm [27] consists in starting from any initial coupling matrix J_{ij}^0 with null entries on the diagonal, and updating recursively the couplings according to

$$\delta J_{ij}^{(d)} = \frac{\lambda}{N} \epsilon_i^{\mu_d} \xi_i^{\mu_d} S_j^{\mu_d}, \quad \delta J_{ii}^{(d)} = 0 \quad \forall i, \quad (11)$$

where λ is a small learning rate, $\mu_d \in [1, \dots, p]$ is a randomly chosen memory index and the mask $\epsilon_i^{\mu_d}$ is defined as

$$\epsilon_i^{\mu_d} = \frac{1}{2} \left(1 - \text{sign} \left(\xi_i^{\mu_d} \sum_{k=1}^N J_{ik} S_k^{\mu_d} \right) \right). \quad (12)$$

In this setting, \tilde{S}^{μ_d} is a noisy memory, generated according to

$$P(S_i^{\mu_d} = x) = \frac{(1 + m_t)}{2} \delta(x - \xi_i^{\mu_d}) + \frac{(1 - m_t)}{2} \delta(x + \xi_i^{\mu_d}). \quad (13)$$

The *training overlap* m_t is a control parameter for the level of *noise* injected during training, corresponding to the expected overlap between \tilde{S}^{μ_d} and $\tilde{\xi}^{\mu_d}$, i.e.

$$m_t = \frac{1}{N} \sum_{j=1}^N \xi_j^{\mu_d} S_j^{\mu_d} + O\left(\frac{1}{\sqrt{N}}\right). \quad (14)$$

Each noisy configuration can be expressed in terms of a vector of *noise units* $\vec{\chi}$, such that

$$S_i^{\mu_d} = \chi_i^{\mu_d} \xi_i^{\mu_d}. \quad (15)$$

In this setting, noise units are i.i.d variables, distributed according to

$$P(\chi_i^{\mu_d} = x) = \frac{(1 + m_t)}{2} \delta(x - 1) + \frac{(1 - m_t)}{2} \delta(x + 1). \quad (16)$$

The algorithm would converge when every configuration with overlap m_t with a memory generates on each site a local field aligned with the memory itself. Let us define the function

$$\mathcal{L}(m, J) = -\frac{1}{\alpha N^2} \sum_{i,\mu}^{N,p} \text{erf} \left(\frac{m \Delta_i^{\mu}}{\sqrt{2(1 - m^2)}} \right). \quad (17)$$

Assuming that stabilities are self-averaging quantities, it can be proven that $-\mathcal{L}(m = m_0, J)$ tends to $m_1(m_0)$ when $N \rightarrow \infty$ [11, 29]. Wong and Sherrington [30, 31]

propose an elegant analysis of a network designed to optimize $\mathcal{L}(m, J)$, i.e. whose couplings J correspond to the global minimum of $\mathcal{L}(m, J)$. Some of their findings, relevant to this work, are:

1. For any m_0 , the maximum value of $m_1(m_0)$ is obtained if $m = m_0$.
2. When $m \rightarrow 1^-$, the minimization of the $\mathcal{L}(m, J)$ trains a linear perceptron with maximal stability, i.e. a SVM.
3. When $m \rightarrow 0^+$, the minimization of $\mathcal{L}(m, J)$ leads to a Hebbian connectivity matrix $J_{ij} \propto J_{ij}^H$.

Eq. 17 is relevant to the TWN procedure, since eq. (11) leads to a reduction of $\mathcal{L}(m, J)$, for any value of m and m_t . In fact, considering a small variation of the stabilities induced by the algorithm update

$$\Delta_i^\mu \rightarrow \Delta_i^\mu + \delta\Delta_i^\mu,$$

and performing a Taylor expansion of (17) at first order in $O(N^{-1/2})$, one obtains (see Appendix A 1)

$$\mathcal{L}' = \mathcal{L} + \sum_{i=1}^N \delta\mathcal{L}_i \quad (18)$$

where

$$\delta\mathcal{L}_i = -\frac{\epsilon_i^{\mu_d} \lambda}{\alpha\sigma_i N^{5/2}} \frac{\sqrt{2}m \cdot m_t}{\sqrt{\pi(1-m^2)}} \exp\left(-\frac{m^2 \Delta_i^{\mu_d}}{2(1-m^2)}\right). \quad (19)$$

Hence, $\delta\mathcal{L}_i$ is strictly non-positive when $\frac{\lambda}{N}$ is small, so that the Taylor expansion is justified. Moreover, we numerically find that iterating (11) with a given value of m_t drives $\mathcal{L}(m = m_t, J)$ to its theoretical absolute minimum computed in [31], as reported in fig. 2 for one choice of N, α and m . This means that the performance of the TWN algorithm can be completely described in the analytical framework of [31] and, that $\mathcal{L}(m = m_t, J)$ can be considered as the loss function optimized by the TWN algorithm. The notation is meant to stress an important differentiation between the two variables m and m_t : the former is a parameter of the loss function, the latter is the level of noise used by the training algorithm. As a technical comment, note that standard deviation along one row of the couplings matrix σ_i (see eq. (2)) is a variable quantity over time, and numerics suggest it is slowly decreasing. As a result, the expansion performed to determine the variation of \mathcal{L} (see eq. (A2) in Appendix A 1) might not be justified after a certain number of steps, leading to a non-monotonic trend of the loss function. The non-monotonic trend of $\mathcal{L}(m = m_t, J)$ due to this effect is showed in the inset of fig. 2. However, this inconvenience can be overcome by rescaling the learning rate λ into $\lambda_i = \lambda \cdot \sigma_i$ at each iteration, as also the curves in fig. 2 display.

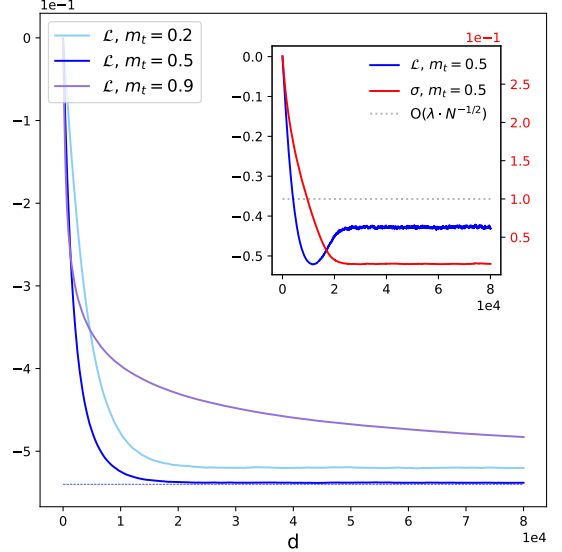


FIG. 2: The *blueish* lines in the main plot report the function $\mathcal{L}(m = 0.5, J)$ for different training overlaps as functions of the number of algorithm steps d . The *dotted* line represents the theoretical minimum value from [31]. The learning strength λ has been rescaled by the standard deviation of the couplings as described in the text. The subplot reports the case $m_t = 0.5$ when the learning strength is not rescaled: \mathcal{L} is in *blue*, while a measure of the standard deviation of the couplings, defined as $\sigma = \frac{1}{N} \sum \sigma_i$, is reported in *red*. The value $\lambda \cdot N^{-1/2}$ is also depicted in *light gray* to properly signal the moment when equation (19) loses its validity. All measures are averaged over 5 realizations of the couplings J . Choice of the parameters: $N = 100$, $\alpha = 0.3$, $\lambda = 1$, the initial couplings are Gaussian with unitary mean, zero variance and $J_{ii}^{(0)} = 0 \forall i$.

A. Classification

The computations contained in [31], and resumed in Appendix B, are now used to calculate n_{SAT} as a function of m_t and α in the TWN problem. The distribution of the stabilities in the trained network (see equation (B4)) has always a tail in the negative values, implying that classification is never reached. The only exception to this statement is the trivial case of $m_t = 1^-$, where $n_{SAT} = 1$ for $\alpha \leq 2$. Nevertheless, the values of n_{SAT} remain close to unity for relatively high values of m_t and relatively low values of α (see fig. 3).

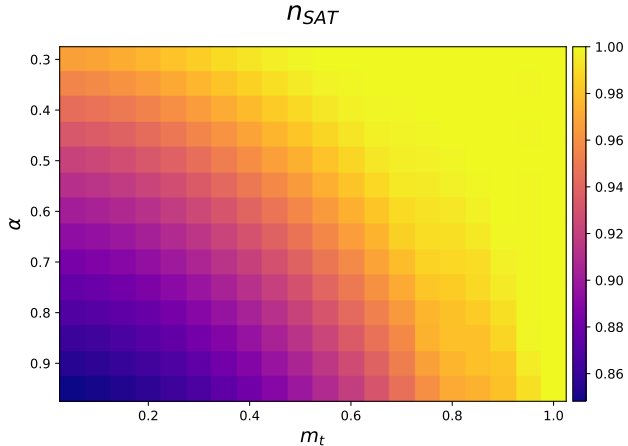


FIG. 3: n_{SAT} as a function of m_t and α . Warmer shades of color are associated to higher classification performances.

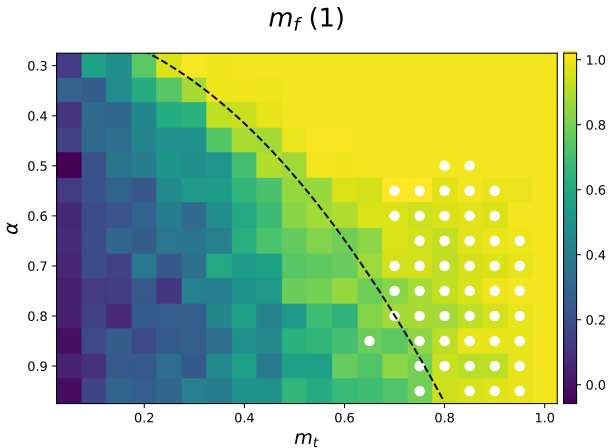


FIG. 4: $m_f(1)$ as a function of m_t and α . Warmer shades of color are associated to higher retrieval performances. The *black dashed* line represents the boundary of the retrieval regime according to the criterion in Appendix C, *white dots* signal the points where basins of attraction to which memories belong are larger than ones obtained from a SVM at $N = 200$.

B. Generalization

The generalization properties of a network trained through TWN are now discussed. The color map in fig. 4 reports the estimate of the retrieval map m_f at $m_0 = 1$ in the limit $N \rightarrow \infty$, i.e. a measure of the distance between a given memory and the closest attractor. Notice

the emergent separation between two regions: one where $m_f(1)$ is mostly smaller than 0.5, and memories are far from being at the center of the basin; another region where $m_f(1)$ is mostly close to unity, i.e. the memory is very close to the center of the basin. Such separation reminds the typical division between *retrieval* and *non retrieval* phases in fully connected neural networks [14], differently from sparse neural networks [31, 32] where the possible topologies of the basins result more various yet harder to get measured by experiments. In Appendix C we propose an empirical criterion to separate these two regions and so limit ourselves to the retrieval one. This criterion is based on assuming that $m_f(m_0)$, measured with respect to the attractor of the basin to which a given memory belongs and not the memory itself, always develops a plateau starting in $m_0 = 1$ when $N \rightarrow \infty$. The behavior of the basin radius is then numerically measured as a function of m_t : when the plateau disappears then one can suppose that basins get shattered in the configurations space due to the interference with the other attractors. The resulting line is reported in fig. 4.

Fixing ourselves to the retrieval region we employ a procedure, also described in Appendix C, to compute the typical size of the basins of attraction. White dots in fig. 4 signal the combinations of (m_t, α) where the basins obtained by TWN algorithm resulted larger than the ones shaped by a SVM at the same value of α . We want to stress the importance of a comparison between the TWN and the relative SVM, since numerical investigations have shown the latter to achieve extremely large basins of attraction, presumably due to the maximization of the stabilities [19, 26]. One can conclude that for most of the retrieval region the generalization performance is worse than the SVM, which maintains larger basins of attraction; on the other hand, at higher values of α the trained-with-noise network sacrifices its classification property to achieve a basin that appears wider than the SVM one. In conclusion, the TWN algorithm never outperforms the relative SVM without reducing its classification capabilities.

III. THE OPTIMAL STRUCTURE OF NOISE

In this section, we study what is the signature of virtuous training configurations for the TWN algorithm. Namely, training configurations leading to a classification regime and a high degree of generalization, resembling the performance of an SVM. It will be helpful for our purposes to implement a symmetric version of rule (11), i.e.

$$\delta J_{ij}^{(d)} = \frac{\lambda}{N} (\epsilon_i^{\mu_d} \xi_i^{\mu_d} S_j^{\mu_d} + \epsilon_j^{\mu_d} \xi_j^{\mu_d} S_i^{\mu_d}). \quad (20)$$

Henceforth in the paper, TWN will be understood as the symmetric update rule contained in eq. (20). Equation (20) can be rewritten explicitly making use of

(12), leading to

$$\delta J_{ij}^{(d)} = \frac{\lambda}{2N} (\xi_i^{\mu_d} S_j^{\mu_d} + S_i^{\mu_d} \xi_j^{\mu_d}) + \frac{\lambda}{2N} (S_i^{1,\mu_d} S_j^{\mu_d} + S_i^{\mu_d} S_j^{1,\mu_d}) \quad (21)$$

where $S_i^{1,\mu_d} = \text{sign} \left(\sum_{k=1}^N J_{ik} S_k^{\mu_d} \right)$. The total update to the coupling at time D can be decomposed as a sum of two contributions

$$\Delta J_{ij}(D) = \Delta J_{ij}^N(D) + \Delta J_{ij}^U(D). \quad (22)$$

The first term on right-hand side, which will be referred to as *noise* contribution, is expressed in terms of noise units as

$$\Delta J_{ij}^N(D) = \frac{\lambda}{2N} \sum_{d=1}^D \xi_i^{\mu_d} \xi_j^{\mu_d} \chi_j^{\mu_d} + \frac{\lambda}{2N} \sum_{d=1}^D \xi_j^{\mu_d} \xi_i^{\mu_d} \chi_i^{\mu_d}, \quad (23)$$

while the second term, which will be referred to as *unlearning* contribution, is given by

$$\Delta J_{ij}^U(D) = -\frac{\lambda}{2N} \sum_{d=1}^D (S_i^{1,\mu_d} S_j^{\mu_d} + S_i^{\mu_d} S_j^{1,\mu_d}). \quad (24)$$

Notice that, in the maximal noise case $m_t = 0^+$, $\Delta J_{ij}^N(D)$ averages to zero over the process. Since its variance is λ/N when the number of steps D is proportional to N/λ , one has

$$\Delta J_{ij}^N(D) = 0^+ + O \left(\sqrt{\frac{\lambda}{N}} \right). \quad (25)$$

A. Characterizing the good training configurations

Section II has shown that the TWN algorithm on fully connected networks never outperforms a SVM without reducing their classification properties. In addition to this, we know from numerics [19, 26] that SVMs, as maximally stable perceptrons, maximize the size of the basins of attraction of the memories. We hence consider the SVMs as optimal recurrent networks in terms of both classification and generalization. As a consequence, to train a well performing neural network one just needs to approach the global minimum of $\mathcal{L}(m = 1^-, J)$. The variation of $\mathcal{L}(m, J)$ can be expressed (see Appendix A 2) as

$$\delta \mathcal{L} = \delta \mathcal{L}_N + \delta \mathcal{L}_U.$$

As detailed in Appendix A 2, in the case of maximal noise (i.e. $m_t = 0^+$) $\delta \mathcal{L}_N$ is negligible, and the only relevant contribution is

$$\delta \mathcal{L}_U \propto \frac{m}{\sqrt{2\pi(1-m^2)}} \sum_{i,\mu}^{N,p} \omega_i^\mu \exp \left(-\frac{m^2 \Delta_i^{\mu^2}}{2(1-m^2)} \right), \quad (26)$$

where ω_i^μ function as weights to the positive Gaussian terms and they are given by

$$\omega_i^\mu = \frac{1}{2\sigma_i} (m_\mu \chi_i^{1,\mu} + m_{1,\mu} \chi_i^\mu), \quad (27)$$

with

$$\chi_i^\mu = \xi_i^\mu S_i^{\mu_d} \quad \chi_i^{1,\mu} = \xi_i^\mu S_i^{1,\mu_d}, \quad (28)$$

and

$$m_\mu = \frac{1}{N} \sum_{j=1}^N S_j^{\mu_d} \xi_j^\mu \quad m_{1,\mu} = \frac{1}{N} \sum_{j=1}^N S_j^{1,\mu_d} \xi_j^\mu. \quad (29)$$

For the case of fixed points, we have $\omega_i^\mu = m_\mu \chi_i^\mu$. When $m \rightarrow 1^-$, the Gaussian terms contained in the sum becomes very peaked around 0. Since we want $\delta \mathcal{L}$ to be negative, we need, for most of the pairs i, μ ,

$$\omega_i^\mu < 0 \text{ when } |\Delta_i^\mu| < 0^+. \quad (30)$$

The more negative ω_i^μ is when $\Delta_i^\mu \sim 0$, the more powerful is its contribution to approach the SVM performances. Selecting training data that satisfy equation (30) amounts to imposing specific internal dependencies among the noise units $\vec{\chi}$, which are no more i.i.d. random variables, as it was in [27]. We refer to such dependencies as *structure* of the noise. One should also bear in mind that training is a dynamic process: to reduce $\mathcal{L}(m = 1^-, J)$ condition (30) should hold during training.

The weights ω_i^μ have a precise geometric interpretation in the case of HU (see also [19]). Define the following N -dimensional vectors: \vec{J}_i as the collection of the elements contained in the i^{th} row of the connectivity matrix, $\vec{\eta}_i^\mu = \xi_i^\mu \vec{\xi}^\mu$ and $\vec{\eta}_i^{\mu_d} = S_i^{\mu_d} \vec{S}^{\mu_d}$, where \vec{S}^{μ_d} is the training configuration. Then, one has $\omega_i^\mu = (\vec{\eta}_i^{\mu_d} \cdot \vec{\eta}_i^\mu)/N$. On the other hand, stabilities can be written as

$$\Delta_i^\mu = \frac{\vec{J}_i \cdot \vec{\eta}_i^\mu}{\sqrt{N} \sigma_i}, \quad (31)$$

and the HU rule becomes

$$\delta \vec{J}_i^{(d)} = -\frac{\lambda}{N} \vec{\eta}_i^{\mu_d}. \quad (32)$$

It follows that, a negative value of ω_i^μ increases the degree of alignment between \vec{J}_i and $\vec{\eta}_i^{\mu_d}$, improving the stability.

B. Position of good training configurations in the energy landscape

The HU algorithm is based on choosing training configurations on a dynamical basis, namely as fixed points of zero temperature dynamics in the energy landscape dictated by Hebb's learning rule. On the

other hand, traditional TWN relies on fully random states, i.e. very high states in the energy landscape. In this section, we generalize this dynamical approach by evaluating the performance of training configurations which lie at different altitudes in the energy landscape of a symmetric neural network, i.e. states that are not limited to be stable fixed points or random states. To do so, we sample training configurations by means of a Monte Carlo routine at temperature T . Temperature acts as a control parameter: when $T = 0$ training configurations are stable fixed points of eq. (1), as in standard HU. Higher values of T progressively reduce the structure of noise in training configurations, and in the limit $T \rightarrow \infty$, training configurations are the same as in the TWN algorithm. The Monte Carlo of our choice is of the Kawasaki kind [33], to ensure that all training configurations are at the prescribed overlap $m_t = 0^+$. We are going to use this technique to probe the states across two types of landscapes: the one resulting from a Hebbian initialization and the one resulting from a SK model [34].

Regarding the Hebbian initialization of the network, numerical results are reported in fig. 5 for four different temperatures. Each panel shows the distribution of $(\Delta_i^\mu, \omega_i^\mu)$. Data points are collected over fifteen realizations of the network, then plotted and smoothed to create a density map. We are interested in the *typical* behavior of ω_i^μ when $\Delta_i^\mu = 0$, which can be estimated by a linear fit of the data. We consider the intercept $\omega_{\text{emp}}(0)$ of the best fit line as an *indicator* of the typical value of ω_i^μ around $\Delta_i^\mu = 0$. We find that at lower temperatures the sampled configurations favor both classification and generalization because $\omega_{\text{emp}}(0)$ is more negative. As temperature becomes too high, $\omega_{\text{emp}}(0)$ gets closer to zero, suggesting low quality in terms of training performance. Numerical observations for progressively increasing values of N suggest that the position of $\omega_{\text{emp}}(0)$ does not change significantly when the size of the system increases, implying that finite size effects are not strong for this kind of measure. One can also study how the distribution of $(\Delta_i^\mu, \omega_i^\mu)$ evolves during the training process. fig. 6a shows the value of $\omega_{\text{emp}}(0)$ at different time steps of the training process, for different values of α , when configurations at $T = 0$ are given to the algorithm. We find that $\omega_{\text{emp}}(0) < 0$ for $\alpha \leq 0.6$. The progressive increase of $\omega_{\text{emp}}(0)$ means that the structure of the fixed points is more effective in the starting Hebbian landscape compared to intermediate stages of training. In the last part of training, points reacquire more negative values, but this is not a reliable indication of good performance: as shown in fig. 6c, in this part of the process the standard deviation of the couplings σ_i is comparable to $O(\lambda \cdot N^{-1/2})$, and the expansion of the \mathcal{L} in eq. (26) is not valid. The last part of the training, where $\sigma_i \simeq 0 \ \forall i$, has been neglected from the plot. The experiment is thus consistent with the characterization of the HU algorithm presented in [19], which showed decreasing classification and

generalization when increasing α . This is confirmed by the study of the Pearson correlation coefficient between ω_i^μ and the associated stabilities Δ_i^μ (see fig. 6b). High values of the Pearson coefficient show a strong dependence of the structure of noise on the relative stabilities. For all α , the Pearson coefficient is highest at $d = 0$, and progressively decreases during training, suggesting that the quality of the training configurations is deteriorating. The final increase in the coefficient is, again, due to the vanishing of the standard deviations σ_i of the couplings, and does not indicate good performance.

For a comparison, one can study the distribution of ω_i^μ in the case of a random initialization of the coupling matrix J . We chose the Sherrington-Kirkpatrick (SK) model [34] as a case of study. Panels (a) and (b) in fig. 7 report the smoothed distribution of $(\Delta_i^\mu, \omega_i^\mu)$ showing a different scenario with respect to the Hebbian one. The distribution looks anisotropic, as in the Hebbian case, yet the stabilities are centered Gaussians, so $\omega_{\text{emp}}(0)$ is positive. In particular, things appear to improve when T increases, in contrast with the previous case of study, though in accordance with the Hebbian limit of the TWN algorithm explained in Section II. Panel (c) displays more clearly the mutual dependence between ω_i^μ and stabilities Δ_i^μ by reporting the Pearson coefficient at the various T between these two quantities: both Hebb's and SK show some mutual dependence, but ω_i^μ and Δ_i^μ in the Hebbian landscape appear to be more correlated. Furthermore, panel (d) shows $\omega_{\text{emp}}(0)$ in both cases. This measure is consistent with the indication coming from the Pearson coefficient: while for the Hebb's initialization $\omega_{\text{emp}}(0)$ remains significantly negative and reaches the lowest values at low temperatures, the random case shows the opposite trend, with the estimated $\omega_{\text{emp}}(0)$ staying generally close to zero.

The role of saddles

Notice, from both panels (c), (d) of fig. 7, the existence of an optimum which does not coincide with the stable fixed points of the dynamics (i.e. $T = 0$). As noted in previous studies on spin glasses [35], one can associate configurations probed by a Monte Carlo at finite temperatures with configurations which are typically saddles in the energy landscape with a given *saddle index*. The *saddle index* is defined as the ratio between the number of unstable sites under the dynamics (see eq. (1)) and the total number of directions N . Stable fixed points have $f = 0$, while random configurations are expected to have $f = 1/2$. In order to check whether a particular f is capturing relevant features of the virtuous training configurations, we sampled training data according to the requirement that their saddle fraction assumes a specific value f and $m_t = 0^+$. Saddles are then employed for training the network according to eq. (11). Sampling is performed by randomly initializing the network on a

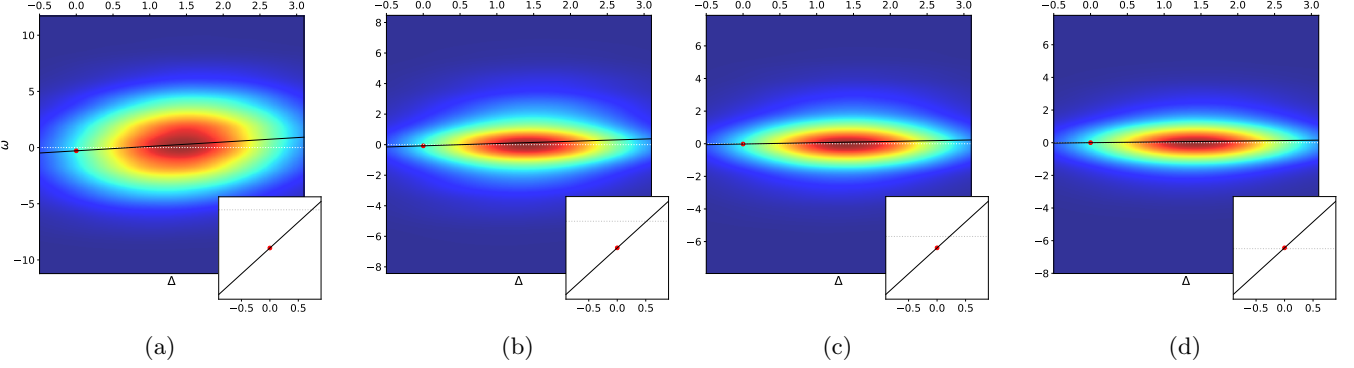


FIG. 5: Distribution of ω_i^μ as a function of Δ_i^μ for training configurations sampled with a Monte Carlo at temperature $T = 0$ i.e. stable fixed points only (a), $T = 0.5$ (b), $T = 1$ (c), $T = 8$ (d), on a Hebbian network. Warmer colors represent denser region of data points. The *full black* line is the non-weighted best fit line for the points, the *dotted white* line represents $\omega = 0$, the *red dot* is the value of the best fit line associated with $\Delta = 0$. Sub-panels to each panel report a zoom of the line around $\Delta = 0$. Measures have been collected over 15 samples of the network. Choice of the parameters: $N = 500$, $\alpha = 0.5$.

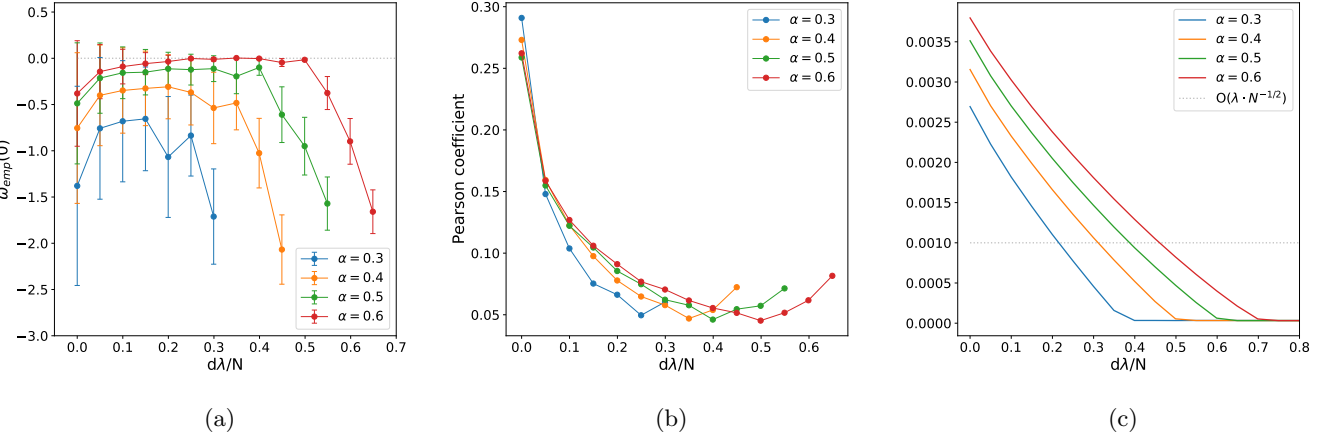


FIG. 6: The TWN algorithm is implemented by sampling stable fixed points of the network dynamics with $m_t = 0^+$. (a) The empirical measure of ω_i^μ around $\Delta_i^\mu = 0$ for the case of stable fixed points as a function of the rescaled number of iterations of the learning algorithm. Errorbars are given by the standard deviations of the measures. (b) Pearson coefficient measured between ω_i^μ and Δ_i^μ . (c) The standard deviation of the couplings during learning, defined as $\sigma = \frac{1}{N} \sum \sigma_i$. Points are averaged over 50 samples and the choice of the parameters is: $N = 100$, $\lambda = 10^{-2}$.

configuration having training overlap $m_t = 0^+$ with a reference memory, and performing a zero temperature dynamics on the landscape defined by the energy

$$E(\vec{S}|f, J) = \frac{1}{2} \left(\frac{1}{N} \sum_{i=1}^N \Theta(-S_i \sum_{j=1}^N J_{ij} S_j) - f \right)^2, \quad (33)$$

where $\Theta(x)$ is the Heaviside function. Yet again, the value of m_t was maintained constant during the descent. The left panel in fig. 8 shows how the minimum stability evolves during the training process while a TWN algorithm is initialized in the Hebbian matrix and learns saddles of different indices. For a network of $N = 100$

and $\alpha = 0.35$, we found that classification is reached until a certain value of f , suggesting that saddles belonging to this band are indeed good training data. The band of saddles that are suitable for learning shrinks when α increases until such states do not significantly satisfy eq. (30) anymore. Such limit capacity is located around the critical one for HU. It should be stressed that the precise performance as a function of f is quite sensitive to the sampling procedure. Simulated annealing routines [36] have also been employed to minimize (33), obtaining qualitatively similar results yet not coinciding with the ones reported in fig. 8. A qualitative study of the basins of attraction of the network has been performed and reported in the right panel in fig. 8. Specifically,

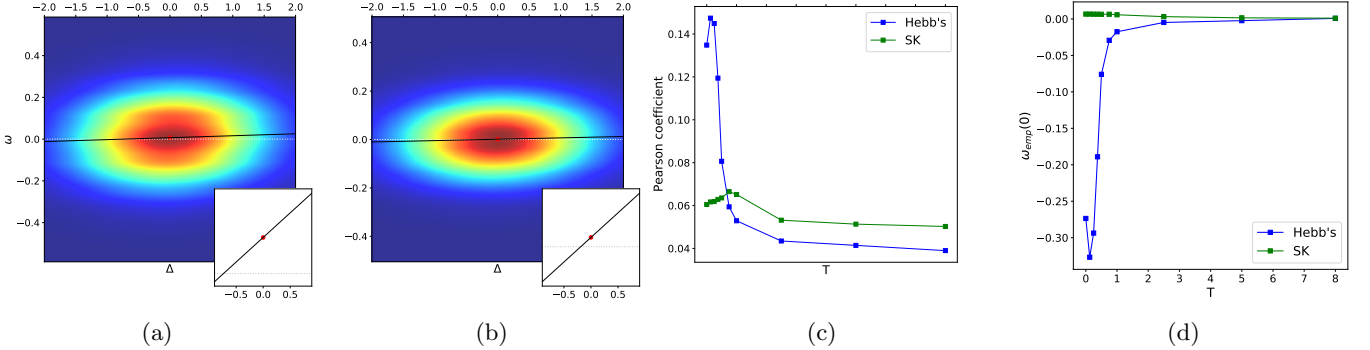


FIG. 7: (a), (b): Distribution of ω_i^μ as a function of Δ_i^μ for training configurations sampled with a Monte Carlo at temperature $T = 0$ i.e. stable fixed points only (a), and $T = 8$ (b) on a SK model. Warmer colors represent denser region of data points. The *full black* line is the non-weighted best fit line for the points, the *dotted white* line represents $\omega = 0$, the *red spot* is the value of the best fit line associated with $\Delta = 0$. Sub-panels to each panel report a zoom of the line around $\Delta = 0$. (c), (d): Comparison between the Hebbian initialization and the Random one through evaluation of: the Pearson coefficient between ω_i^μ and Δ_i^μ (c) and the estimated value of $\omega_{emp}(0)$ from the dispersion plots (d). Measures have been collected over 15 samples of the network. Choice of the parameters: $N = 500$, $\alpha = 0.5$.

the retrieval map $m_f(m_0)$ has been measured relatively to the saddle indices f at the first time they reached classification, in analogy to what has been measured in [19]. The curves coincide quite well, suggesting that finite sized networks trained with different f assume similar volumes of the basins of attraction when they are measured at the very first instant they reach classification. The plot also shows that the generalization performance is comparable with the one of a SVM trained with the same choice of the control parameters.

IV. STABLE FIXED POINTS AS NOISY TRAINING DATA

Motivated by the results of the previous sections on the characterization of effective training configuration, we select training configurations for the TWN algorithm which are not only characterized by a fixed value of overlap with the memories m_t , but are also fixed points of the dynamics, after initializing the coupling according to Hebb's rule. We firstly evaluate the maximal noise case $m_t = 0^+$, where the considerations of Section III A apply, and then move to $m_t > 0^+$.

A. Maximal noise case: $m_t = 0^+$

As mentioned in Section III, in this case the only relevant contribution to the update rule is

$$\Delta J_{ij}^U(D) = -\frac{\lambda}{N} \sum_{d=1}^T S_i^{\mu_d} S_j^{\mu_d}, \quad (34)$$

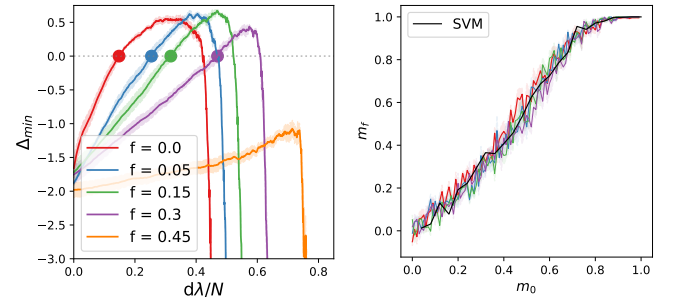


FIG. 8: Left: Minimum stability Δ_{min} as a function of the algorithm steps on a network trained with the TWN routine that learns saddles of various indices f . The initial matrix is assembled according to the Hebb's rule. Full dots report the amount of iterations needed to accomplish classification. Right: the retrieval map $m_f(m_0)$ as measured on the positions of the colored dots from the right panel, with the same color code being applied. A comparison with a SVM trained with the same choice of the parameters is also presented through the *dashed blue* line. All measures are averaged over 5 samples with the shaded region indicating the experimental errors. The choice of the parameters is: $N = 100$, $\alpha = 0.35$, $\lambda = 10^{-3}$.

which is the classic HU update rule. As a result, when $\lambda/N \rightarrow 0$ the TWN algorithm and the HU algorithm will converge to the same updating rule for the couplings when stable fixed points of the dynamics are used in the training. The same argument can be applied to the original asymmetric rule (11), however asymmetric networks may have no stable fixed points of (1) that can be eas-

ily reached to be learned. We now perform a numerical test of the argument above, in the case of a symmetric connectivity matrix. At each step of the algorithm, the network is initialized with an initial overlap contained in $(0, N^{-1/2})$ with one memory $\vec{\xi}^{\mu_d}$. Then, asynchronous dynamics (1) is run until convergence, and the final overlap m_t is measured. If $m_t \in (0, N^{-1/2})$, we use the sampled configuration for training, otherwise the process is repeated. Typically, an initial overlap equal to 0^+ implies a similar order of magnitude for the final overlap, hence no reiteration is needed. The algorithm (20) is repeated for $D^* = O(N/\lambda)$ steps. The order of magnitude of $\Delta J_{ij}^U(D)$ is supposed to be the same of $J_{ij}^{(0)}$, in order to see significant modifications to the initial connectivity matrix. The network is initialized according to the Hebb's rule (6), i.e. $J_{ij}^{(0)} = O(N^{-1/2})$ which implies $\Delta J_{ij}^U(D) = O(N^{-1/2})$ at leading order. The contributions U and N are compared by computing the norm of the relative ΔJ matrix and evaluating the ratio $|\Delta J^U|/|\Delta J^N|$. From our previous considerations we expect $|\Delta J^U|/|\Delta J^N|$ to be linear in $\lambda^{-1/2}$ when corrections vanish. Results are reported in fig. 9: $|\Delta J^U|/|\Delta J^N|$ grows when N increases and λ decreases, according to the scaling relation predicted by our argument. In addition to this, curves are collapsing on the expected line when $\lambda \rightarrow 0$ and $N \rightarrow \infty$.

We also measured Δ_{\min} at its maximum over the course of the algorithm (as described in Section IB 3). Results are reported in fig. 10. Δ_{\min} produced by TWN and HU are found to coincide when λ is sufficiently low. Moreover, the number of steps necessary to reach the maximum are the same for both the algorithms, confirming that couplings are transforming in the same way. This last aspect is corroborated by the subplot in fig. 10, representing the set of J_{ij} obtained with the traditional HU algorithm as a function of the ones resulting from the TWN algorithm, for one realization of the network. The strong correlation is evident, as predicted from our arguments.

B. General noise case: $m_t > 0^+$

When training configurations are fixed points of the dynamics with $m_t > 0^+$, the considerations of the previous section no longer apply. Such configurations can be generated by initializing the network at an overlap $m > 0^+$ with a memory, and let it evolve according to (1). The connectivity matrix is initialized according to Hebb's learning rule eq. (6). In this setting, if at some point during training m happens to enter the basin of attraction of the memories, the fixed point reached by the dynamics will be the memory itself, and the noise contribution will cancel exactly the learning contribution, giving $\delta J = 0$. On the other hand, for sufficiently high values of the load α , at the start of the training procedure memories will have zero size basins of attraction and trajectories will

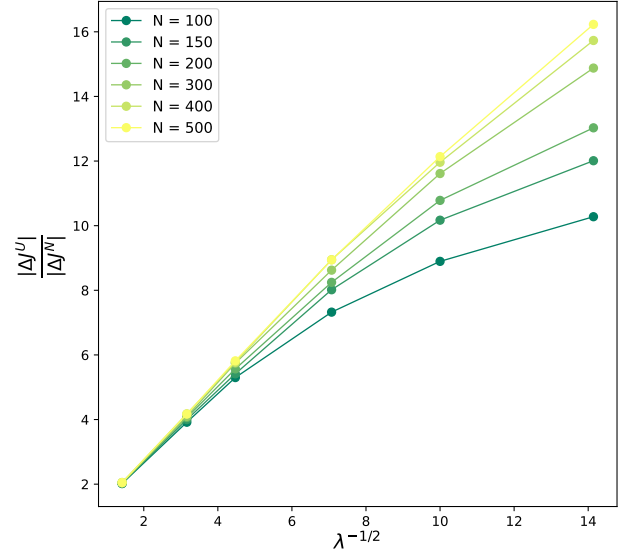


FIG. 9: Estimates of the ratio $|\Delta J^U|/|\Delta J^N|$ as a function of $\lambda^{-1/2}$ and N for $\alpha = 0.5$. Measures are averaged over 5 samples. Error bars are not indicated because smaller than the symbols.

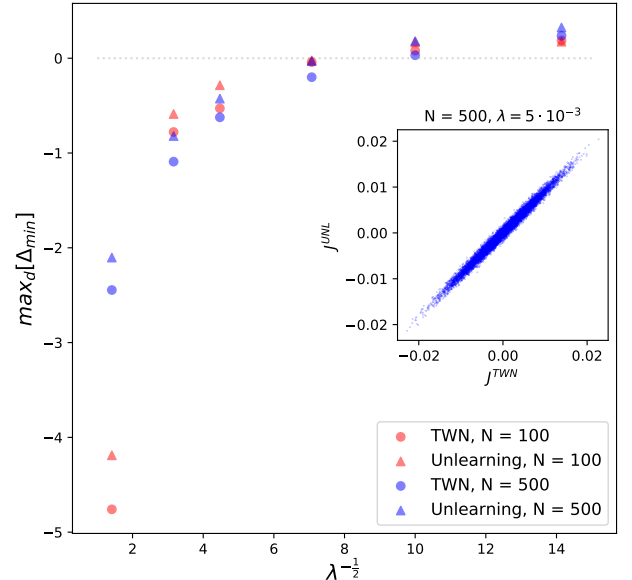


FIG. 10: The quantity $\max_d(\Delta_{\min})$ as a function of $\lambda^{-1/2}$. Colors are: *red* for $N = 100$ and *blue* for $N = 500$. The *gray* line represents the null value for the stability. Symbols are: *circles* for the TWN rule, *triangles* for the HU rule. In the subplot on the center right, the couplings obtained through the HU algorithm are plotted as a function of the ones resulting from the TWN, at the same amount of iterations, for one sample at $N = 500$ and $\lambda = 5 \cdot 10^{-3}$. Measures are averaged over 50 samples. The choice of the parameters is: $\alpha = 0.5$, $m_t = 0^+$ for TWN.

drift away from the memories following the dynamics. In this scenario, the two contributions δJ^N and δJ^U decorrelate, and δJ^N will take again a similar role to what described in the previous section. The result is an algorithm which interpolates between HU when d is small and a supervised algorithm when basins increase to a size close to $(1 - m)$. In this regime, δJ^N acts as a breaking term, preventing the algorithm to further modify the coupling matrix J . A similar mechanism has been studied in [37] where a supervised term was added to the standard HU update rule, leading to $\delta J_{ij} \propto -S_i^{\mu_d} S_j^{\mu_d} + \xi_i^{\mu_d} \xi_j^{\mu_d}$. Notice that the term $\xi_i^{\mu_d} \xi_j^{\mu_d}$ is deterministically reproducing Hebb's learning rule, while in our study the HU is modified by a stochastic term, whose nature we have already discussed. Given a sufficiently small learning rate λ , there will exist a characteristic number of steps of the algorithm over which the coupling matrix does not change significantly. We will call this timescale *an epoch*. Averaging the effect of training steps over an epoch, we get a snapshot of how the algorithm is affecting the couplings at a given point during training. This can be used to study the relation between δJ^N and δJ^U , quantified by the connected correlation coefficient

$$\text{Cov}_{N-U} := \frac{2}{N(N-1)} \sum_{i,j>i} (\overline{\delta J_{ij}^N \delta J_{ij}^U} - \overline{\delta J_{ij}^N} \overline{\delta J_{ij}^U}), \quad (35)$$

where the average is computed over an epoch. When this quantity equals one, there is no effective update of the couplings over an epoch. Results are presented in fig. 11 for different values of m and of α , as a function of the number of training steps d . The number of iterations has been rescaled by a factor p/λ for clarity of the plot. At any given α , training with higher m results in a faster increase of Cov_{N-U} , i.e. a faster convergence of the algorithm. If the value of m is too low, the algorithm never manages to build a big enough basin of attraction, and never stops. As α is increases, higher and higher values of m are required for the algorithm to stop, since the typical size of the attraction basins shrinks.

The network performance can be benchmarked by tracking the evolution of the lowest stability Δ_{\min} throughout the training procedure. Results are presented in fig. 12 for different values of α and m . For sufficiently low values of α and sufficiently high values of m , Δ_{\min} surpasses the zero. Once this condition is met, the value Δ_{\min} becomes essentially constant, even if $\text{Cov}_{N-U} < 1$, signaling that the update of the coupling matrix is still in progress. The result is a curve $\Delta_{\min}(d)$ which barely surpasses zero. For each value of m there exists a critical value $\alpha_c(m)$ beyond which no amount of steps is able to produce $\Delta_{\min} > 0$. Extrapolating empirical results to the $N \rightarrow \infty$ limit, one finds

$$\alpha_c(m) = A \cdot (m)^B + C,$$

where

$$A = 0.35 \pm 0.01, \quad B = 6.9 \pm 0.5, \quad C = 0.58 \pm 0.01$$

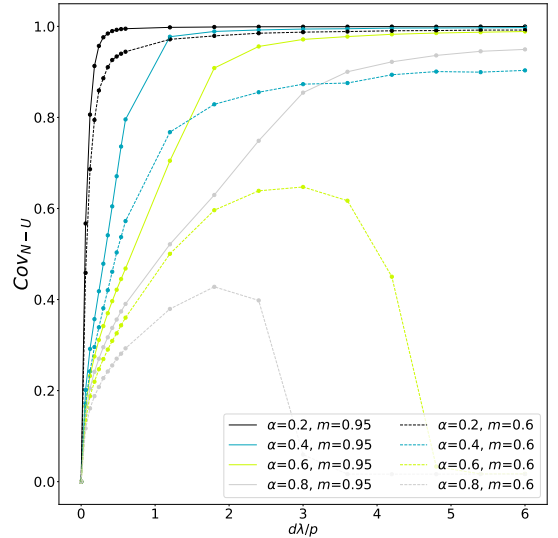


FIG. 11: Correlation between *noise* and *unlearning* contributions to δJ as a function of the rescaled number of training steps $\frac{d\lambda}{p}$, for two values of the training parameter m , and different values of α . When $\text{Cov}_{N-U} = 1$, the algorithm stops modifying the coupling matrix. Results are averaged over 100 samples. Choice of the parameters: $N = 400$, $\lambda = 10^{-2}$.

Consistently with what presented in the previous section, in the limit $m \rightarrow 0^+$ one finds the critical capacity of the HU algorithm [19, 23]. The critical capacity increases up to a value $\alpha_c(1) = 0.93 \pm 0.01$ when m reaches unity.

Regardless of whether $\Delta_{\min} > 0$ is obeyed, one can monitor the network performance as an associative memory device by measuring the retrieval map $m_f(m_0)$. We find that the best performance always corresponds to the number of training step maximizing Δ_{\min} , hence the curves $m_f(m_0)$ are all relative to this number of steps. Results are presented in fig. 13. When classification is achieved (i.e. $\alpha < \alpha_c(m)$), lower values of m increase the degree of generalization of the network (i.e. enlarge the basins of attraction), at the cost of a lower critical capacity.

V. SAMPLING THE OPTIMAL NOISE

Insights from the previous sections on the characterization of well performing training data can be used to design algorithms that only use such good data. Namely, one can use a supervised Monte Carlo routine that searches for maximally noisy configurations (i.e. $m_t = 0^+$) satisfying condition (30). In our new algorithm, the coupling matrix is initialized according to Hebb's rule (6), and updated recursively on the basis of the cleverly sampled training data, according to either TWN eq. (20) or HU eq. (9). We first introduce the sampling algorithm and then report some numerical results

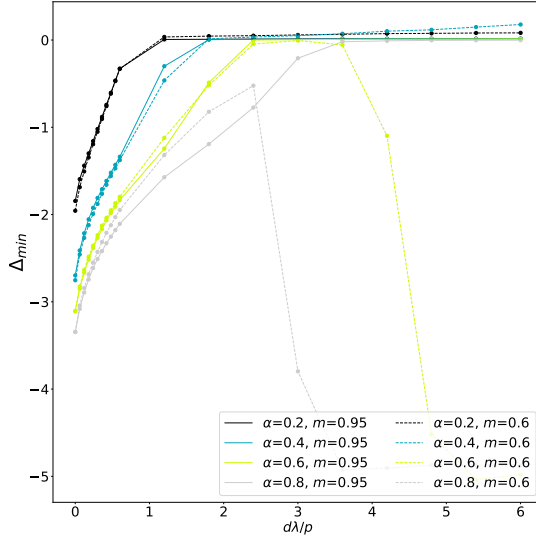


FIG. 12: Minimum stability as a function of the rescaled number of training steps $\frac{d\lambda}{\lambda}$, for two values of the training parameter m , and different values of α . When $\Delta_{\min} \geq 0$, each memory is a stable fixed point of the dynamics. Results are averaged over 100 samples.

Choice of the parameters: $N = 400$, $\lambda = 10^{-2}$.

regarding both the TWN and HU routines.

A. The sampling algorithm

We sample maximally noisy training configurations $m_t = 0^+$ such that $E(\vec{\chi}|m, J) < 0$, where

$$E(\vec{\chi}|m, J) := \frac{m}{\sqrt{2\pi(1-m^2)}} \sum_{i,\mu}^{N,p} \omega_i^\mu \exp\left(-\frac{m^2 \Delta_i^\mu}{2(1-m^2)}\right), \quad (36)$$

that is a function of the noisy variables χ_i^μ , conditioned on a reference overlap m and the couplings J . Sampling is done through the following procedure:

1. The network is initialized in a random configuration and the asynchronous dynamics in eq. (1) is run until convergence on a fixed point. The final state \vec{S}^{μ_d} must have an overlap m_t in the interval $(0, 1/\sqrt{N})$ with one memory μ_d , otherwise the procedure is repeated.
2. A $T = 0$ temperature dynamics in the landscape of $E(\vec{\chi}|m, J)$ is performed until $E(\vec{\chi}|m, J) < 0$. We use a Kawasaki kind of dynamics over the noisy variables $\vec{\chi}$ to make sure that m_t maintains the prescribed value.

Since $E(\vec{\chi}|m, J)$ is proportional to $\delta\mathcal{L}_U$ (see eq. (26)), the procedure will lead to a reduction in the Loss in eq. (17). In this setting, the classification and generalization properties can be tuned by the parameter m , while the training configurations always have a fixed value of $m_t = 0^+$.

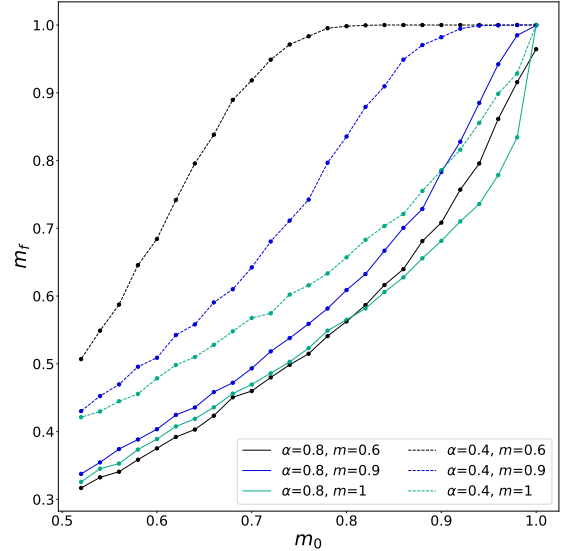


FIG. 13: Retrieval map $m_f(m_0)$ for two values of α and different values of the training parameter m . At $\alpha = 0.4$, every m leads to stable memories, i.e. $m_f(1) = 1$. At $\alpha = 0.8$, only the highest values of m lead to stable memories, while for low values of m one has $m_f(1) < 1$. Results are averaged over 100 samples. Choice of the parameters: $N = 400$, $\lambda = 10^{-2}$.

In particular, to require a performance that is most similar to the one of a SVM, we will set $m \rightarrow 1^-$.

The sampling procedure starts from fixed points because we know, from the previous sections, that they are close to be the most effective configurations. Interestingly, the described procedure results significantly more effective than a standard minimization of $\mathcal{L}(m = 1^-, J)$: in the latter case training stops when $\mathcal{L} = -1$, while the former technique apparently pushes the stabilities further in the positive values.

B. Algorithm performance

The sampling procedure results in a better performance for both TWN and the HU update rules. Results for TWN are reported in fig. 14. Panel (a) shows that classification is reached up to $\alpha \simeq 0.8$ for a network of size $N = 100$. Panel (b) shows the retrieval map $m_f(m_0)$, for different values of α and for the lowest number of algorithm iterations leading to classification. The high values of m_f for $m_0 \sim 1$ indicates that the network, while achieving classification, maintains good generalization properties. Results for a SVM with the same control parameters are also shown, for comparison. The curves obtained from TWN are higher than ones relative to the SVM, signaling a better recalling performance, even though quantifying this effect will require a more detailed study of finite size effects. Fig. 15 shows analogous plots for the HU update rule. Again, the network

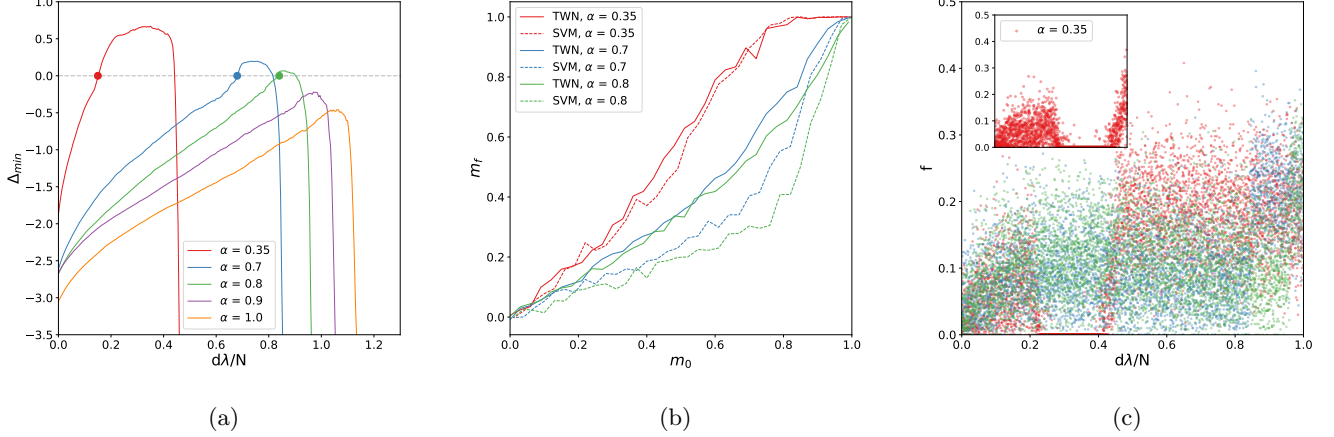


FIG. 14: Performance of the TWN algorithm taught with noisy configurations sampled according to Section V regarding four progressing values of the load α . (a) Minimum stability as a function of the algorithm time: *full* line is the HU with sampling, *dotted* line is the traditional HU. (b) Retrieval map $m_f(m_0)$, relatively to the *circles* in panel (a) for $\alpha \in [0.35, 0.7, 0.8]$: *full* line is the HU with sampling, *dashed* line is a SVM trained with no symmetry constraints with the same control parameters. (c) Saddle index f as a function of the algorithm steps for $\alpha \in [0.35, 0.7, 0.8]$. The sub-panel zooms over $\alpha = 0.35$ alone. All data points have been averaged over 20 samples in (a),(b) and 5 samples in (c). Errors are neglected for clarity of the image. The choice of the parameters: $N = 100$, $\lambda = 10^{-3}$, $m = 0.9999$.

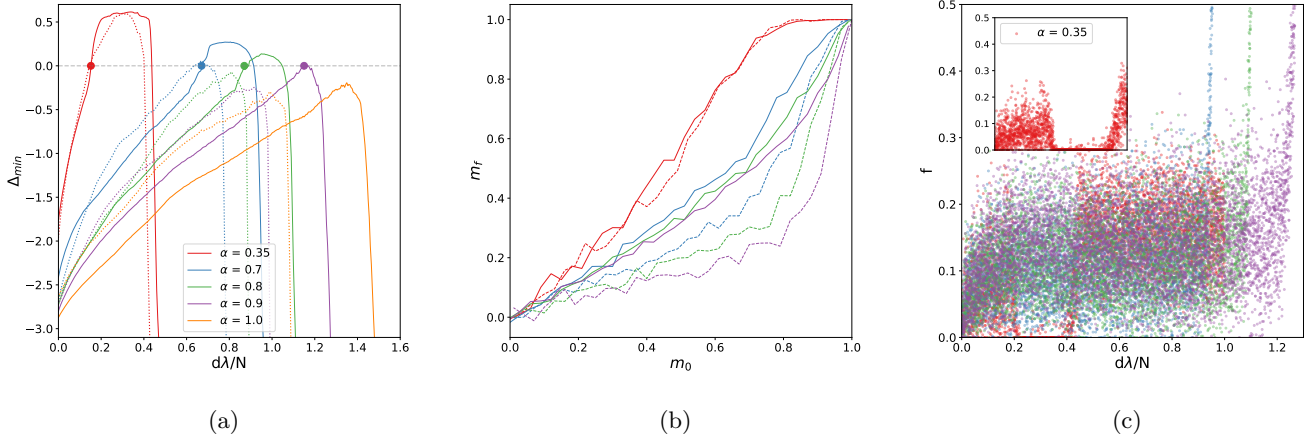


FIG. 15: Performance of the HU algorithm trained with noisy configurations sampled according to Section V regarding four progressing values of the load α . (a) Minimum stability as a function of the algorithm time: *full* line is HU with sampling, *dotted* line is the traditional HU. (b) Retrieval overlap $m_f(m_0)$, relatively to the *circles* in panel (a) for $\alpha \in [0.35, 0.7, 0.8, 0.9]$: *full* line is HU with sampling, *dashed* line is a SVM trained with no symmetry constraints with the same control parameters. (c) Saddle index f as a function of the algorithm steps for $\alpha \in [0.35, 0.7, 0.8, 0.9]$. The sub-panel zooms over $\alpha = 0.35$ alone. All data points have been averaged over 20 samples in (a),(b) and 5 samples in (c). Errors are neglected for clarity of the image. The choice of the parameters: $N = 100$, $\lambda = 10^{-3}$, $m = 0.9999$.

compares favorably with traditional HU in terms of memory capacity, that is increased up to $\alpha \simeq 0.9$ (see panel (a)) with respect to the maximum capacity of $\alpha \simeq 0.7$ obtained with fixed points only. Panel (b) represents an indication for the sizes of the basins of attraction at the

lowest number of algorithm iterations leading to classification. Yet again basins appear to be larger than the ones from a SVM trained with the same control parameters.

Panel (c) in fig. 14 and fig. 15 report the behavior of the

saddle index f of the sampled configurations as a function of the number of steps of the algorithm, relatively to TWN and HU respectively. Most of the sampled training configurations are low index saddles. When α is low, there exists an interval in the training process when stabilities are all far above zero. During this interval, the exponential factors in eq. (36) are all extremely small, resulting in negligible improvement of the loss function regardless of the training configuration chosen by the sampler. Correspondingly, the sampler contents itself with fixed points of the dynamics, resulting in the gap in the saddle bands visible in the insets of fig. 14 and fig. 15 (c) for $\alpha = 0.35$. For higher values of α , i.e. when the training task is more challenging, the algorithm never succeeds to increase Δ_{min} to the point of making sampling trivial, and there is no gap in the saddle band.

VI. CONCLUSIONS

Gardner's seminal work [27] showed that noise could be injected during training to increase generalization, i.e. the capability of neural networks to retrieve classes of data by receiving corrupted stimuli [6, 38–40]. The same concept recently seems to catch on in biology as well [41, 42], as artificial neural networks appear more frequently to be involved in explaining neuroscience, and viceversa.

In our work, as detailed in Section II, we showed that the training-with-noise algorithm (TWN) [27] is well described by Wong and Sherrington's calculations in [30, 31]. This implies convergence to a Hebbian matrix [12, 14] (see Section IB 1) or a Support Vector Machine (SVM) [9, 20, 43] (see Section IB 2) when learning random configurations with, respectively, a maximal (i.e. $m_t = 0^+$) and a minimal (i.e. $m_t = 1^-$) amount of noise. The training overlap m_t can be then tuned to interpolate between these two models. The emergent performance of the network trained in this way is a consequence of the choice of a i.i.d. noise, generated according to a binomial generation process.

In Section III we considered the maximal noise scenario, i.e. $m_t = 0^+$, and derived the condition for the noise to be satisfied to train a SVM. Specifically, the entries of training configurations are constrained to show particular internal dependencies that we call *structure*. At each step of the TWN algorithm we define a set of variables ω_i^μ , depending on both the training data and the stabilities of the network at that time step, and we require them to be typically negative when $\Delta_i^\mu \sim 0$. The more they are negative in this narrow range, the more effective the data point is in leading to classification and good generalization. In this framework, the shape of the initial landscape of attractors where configurations are sampled assumes a crucial role. We find that the Hebbian landscape in the *oblivion* regime (i.e. $\alpha > \alpha_c^H$) is a very effective starting condition for learning. In fact, our analysis, based on running a Monte Carlo at finite temperature through

the energy function, shows that the quality of the configurations, in terms of noise structure, increases when we descend towards the metastable minima of a Hebbian landscape, by contrast with what is observed in a fully random landscape. By observing that states sampled by a Monte Carlo at finite temperature are typically saddles of a certain saddle index (i.e. number of unstable directions according to the neural dynamics) we test the existence of a band of prolific maximally noisy saddle states in the lower levels of a Hebbian landscape. Such states are able to train a system which shares the same properties of a SVM.

In Section IV we analyzed the particular case of noisy training data that are also stable fixed points of the dynamics. We firstly proved that the traditional HU algorithm [19, 22–24] described in Section IB 3 is recovered from the TWN algorithm when the noise is maximal and the training configurations are stable fixed points of the dynamics. Therefore, it is now clear why basins of attraction are close to be maximized by the HU algorithm as displayed by [19]: training data are such as to approach the global minimum of the loss function of a SVM. The same 'unlearning' principle is traditionally applied by other unsupervised procedures such as [44–47]. However, these algorithms learn configurations that are higher in the landscape of attractors. Consistently with our study, such techniques achieve small or nonexistent basins of attraction, while the traditional HU routine, that makes use of the metastable states, approaches an optimal memory performance. In addition to the maximal noise scenario, we studied an application of the TWN algorithm when stable fixed points with $m_t > 0^+$ are learned by the network, as it is initialized according to the Hebb's rule. The resulting algorithm reaches both classification and a good degree of generalization, proving that the internal structure of the configurations plays a relevant role also for higher values of m_t . The critical capacity reached by the algorithm has been numerically estimated.

Eventually, Section V introduced a sampling algorithm for effective training data, i.e. the configurations of the landscape that can be used both in the TWN and HU algorithms to approach the SVM performance. We find that such a procedure can be employed to outperform the traditional HU algorithm both in terms of critical capacity and basins of attraction.

As neuroscientists become more convinced of the importance of sleep in memory consolidation [48, 49], various connections seem to arise between unsupervised training algorithms on machines and synaptic plasticity processes that occur outside the wakeful hours [21, 50–52]. In light of these remarks and the work presented in this article, one might conceive natural learning as a *two-phase* process. During a first *online* phase external stimuli are processed by the network through the standard training-with-noise algorithm. One can imagine the stimuli to be maximally noisy versions of some unknown *archetypes* embedded into the environment. As a con-

sequence, training will shape a pure Hebbian landscape of attraction out of the retrieval regime. In a second *offline* phase, the early formed network samples structured noisy neural configurations, still weakly correlated with the archetypes, from the landscape of attractors. Such states could be, for instance, lower saddles or stable fixed points of the neural dynamics. These neural configurations are then processed by the same kind of training-with-noise algorithm, and memory is consolidated by centering the unconscious archetypes in the middle of large basins of attraction.

In this context, the results contained in this work make progress on two fronts. On one side, they shed light over the structure of noise that is optimal for learning in neural networks, helping to develop a finer theory behind the very empirical techniques of noise injection implemented

in training deep networks [6, 7, 53, 54]. On the other side, they draw a connection between unsupervised, and thus more biologically relevant, learning processes and the supervised ones, from which most of the modern theory of neural networks derive. Hence, our results encourage an in-depth study of the noise, and its structure, used by the brain to effectively shape associative memory.

ACKNOWLEDGMENTS

The authors are particularly grateful to their mentors Enzo Marinari, Giancarlo Ruocco and Francesco Zamponi for precious suggestions and support. They also thank Fabian Aguirre Lopez, Aldo Battista, Simona Cocco, Giampaolo Folena, Rémi Monasson and Mauro Pastore for useful discussions.

[1] D.J. Amit. *Modeling Brain Function*. Cambridge University Press, 1989.

[2] M. Mezard, G. Parisi, and M. Virasoro. *Spin Glass Theory and Beyond: An Introduction to the Replica Method and Its Applications*, volume 9 of *World Scientific Lecture Notes in Physics*. World Scientific, 1986.

[3] Alex Labach, Hojjat Salehinejad, and Shahrokh Valaei. Survey of Dropout Methods for Deep Neural Networks, 2019. arXiv:1904.13310.

[4] A. Achille and S. Soatto. Information dropout: Learning optimal representations through noisy computation. *IEEE transactions on pattern analysis and machine intelligence*, 40(12):2897–2905, 2018.

[5] H. Noh, T. You, J. Mun, and B. Han. Regularizing deep neural networks by noise: Its interpretation and optimization. *Advances in neural information processing systems*, 30, 2017.

[6] N. Srivastava, G. Hinton, A. Krizhevsky, I. Sutskever, and R. Salakhutdinov. Dropout: A simple way to prevent neural networks from overfitting. *Journal of Machine Learning Research*, 15:1929, 2014.

[7] C. Shorten and T. M. Khoshgoftaar. A survey on Image Data Augmentation for Deep Learning. *Journal of Big Data*, 6(1):1, 2019.

[8] L. Zhao, T. Liu, X. Peng, and D. Metaxas. Maximum-Entropy Adversarial Data Augmentation for Improved Generalization and Robustness. In *Advances in Neural Information Processing Systems*, volume 33, pages 14435–14447. Curran Associates, Inc., 2020.

[9] E. Gardner. The space of interactions in neural network models. *Journal of Physics A: Mathematical and General*, 21(1):257, 1988.

[10] M. Minsky and P. Seymour. *Perceptrons: an introduction to computational geometry*. MIT Press, 1969.

[11] T.B. Kepler and L.F. Abbott. Domains of attraction in neural networks. *Journal de Physique*, 49(10):1657, 1988.

[12] J.J. Hopfield. Neural networks and physical systems with emergent collective computational abilities. *Proceedings of the National Academy of Sciences*, 79(8):2554, 1982.

[13] D.O. Hebb. *The Organization of Behavior: A Neuropsychological Theory*. John Wiley and Sons, 1949.

[14] D. J. Amit, H. Gutfreund, and H. Sompolinsky. Storing Infinite Numbers of Patterns in a Spin-Glass Model of Neural Networks. *Physical Review Letters*, 55(14):1530, 1985.

[15] E. Gardner, H. Gutfreund, and I. Yekutieli. The phase space of interactions in neural networks with definite symmetry. *Journal of Physics A: Mathematical and General*, 22(12):1995, 1989.

[16] A. Battista and R. Monasson. Capacity-resolution trade-off in the optimal learning of multiple low-dimensional manifolds by attractor neural networks. *Physical Review Letters*, 124(4):048302, 2020.

[17] N. Brunel, V. Hakim, P. Isopi, J.P. Nadal, and B. Barbour. Optimal Information Storage and the Distribution of Synaptic Weights: Perceptron versus Purkinje Cell. *Neuron*, 43(5):745–757, 2004.

[18] N. Brunel. Is cortical connectivity optimized for storing information? *Nature Neuroscience*, 19(5):749–755, 2016.

[19] M. Benedetti, E. Ventura, E. Marinari, G. Ruocco, and F. Zamponi. Supervised perceptron learning vs unsupervised Hebbian unlearning: Approaching optimal memory retrieval in Hopfield-like networks. *The Journal of Chemical Physics*, 156(10):104107, 2022.

[20] B. Schölkopf and A.J. Smola. *Learning with Kernels: Support Vector Machines, Regularization, Optimization, and Beyond*. The MIT Press, 2018.

[21] F. Crick and G. Mitchison. The function of dream sleep. *Nature*, 304(5922):111, 1983.

[22] J.J. Hopfield, D.I. Feinstein, and R.G. Palmer. ‘Unlearning’ has a stabilizing effect in collective memories. *Nature*, 304(5922):158, 1983.

[23] J.L. Van Hemmen, L.B. Ioffe, R. Kühn, and M. Vaas. Increasing the efficiency of a neural network through unlearning. *Physica A: Statistical Mechanics and its Applications*, 163(1):386, 1990.

[24] J.L. van Hemmen and N. Klemmer. Unlearning and Its Relevance to REM Sleep: Decorrelating Correlated Data. In J.G. Taylor, C.L.T. Mannion, J.G. Taylor, E.R. Caianiello, R.M.J. Cotterill, and J.W. Clark, editors, *Neural Network Dynamics*, page 30. Springer London, London, 1992.

[25] E. Gardner. Structure of metastable states in the Hopfield model. *Journal of Physics A: Mathematical and General*, 19(16):L1047, 1986.

[26] B.M. Forrest. Content-addressability and learning in neural networks. *Journal of Physics A: Mathematical and General*, 21(1):245, 1988.

[27] E. J. Gardner, D. J. Wallace, and N. Stroud. Training with noise and the storage of correlated patterns in a neural network model. *Journal of Physics A: Mathematical and General*, 22(12):2019, 1989.

[28] Y. Le Cun. Learning Process in an Asymmetric Threshold Network. In *Disordered Systems and Biological Organization*, page 233. Springer, Berlin, Heidelberg, 1986.

[29] E. Gardner. Optimal basins of attraction in randomly sparse neural network models. *Journal of Physics A: Mathematical and General*, 22(12):1969, 1989.

[30] K.Y.M. Wong and D. Sherrington. Optimally adapted attractor neural networks in the presence of noise. *Journal of Physics A: Mathematical and General*, 23(20):4659, 1990.

[31] K.Y.M. Wong and D. Sherrington. Neural networks optimally trained with noisy data. *Physical Review E*, 47(6):4465, 1993.

[32] B. Derrida, E. Gardner, and A. Zippelius. An Exactly Solvable Asymmetric Neural Network Model. *Europhysics Letters (EPL)*, 4(2):167, 1987.

[33] M. Newman and G. Barkema. *Monte Carlo Methods in Statistical Physics*. Oxford University Press, 1999.

[34] D. Sherrington and S. Kirkpatrick. Solvable Model of a Spin-Glass. *Physical Review Letters*, 35(26):1792, 1975.

[35] T. Aspelmeier, R.A. Blythe, A.J. Bray, and M.A. Moore. Free energy landscapes, dynamics and the edge of chaos in mean-field models of spin glasses. *Physical Review B*, 74(18):184411, 2006.

[36] S. Kirkpatrick, C.D. Gelatt, and M.P. Vecchi. Optimization by simulated annealing. *Science*, 220(4598):671, 1983.

[37] G. Pöppel and U. Krey. Dynamical Learning Process for Recognition of Correlated Patterns in Symmetric Spin Glass Models. *Europhysics Letters*, 4(9):979, 1987.

[38] T. Tadros, G. Krishnan, R. Ramya, and Bazhenov M. Biologically inspired sleep algorithm for increased generalization and adversarial robustness in deep neural networks. *International Conference on Learning Representations*, 2019.

[39] D. Saad and S. Solla. Learning with Noise and Regularizers in Multilayer Neural Networks. In *Advances in Neural Information Processing Systems*, volume 9. MIT Press, 1996.

[40] B. Schottky and U. Krey. Phase transitions in the generalization behaviour of multilayer perceptrons: II. The influence of noise. *Journal of Physics A: Mathematical and General*, 30(24):8541, 1997.

[41] E. Hoel. The overfitted brain: Dreams evolved to assist generalization. *Patterns*, 2(5):100244, 2021.

[42] F. Stella, P. Baracskay, J. O'Neill, and J. Csicsvari. Hippocampal Reactivation of Random Trajectories Resembling Brownian Diffusion. *Neuron*, 102(2):450, 2019.

[43] S. Diamond and S. Boyd. CVXPY: A Python-Embedded Modeling Language for Convex Optimization. *Journal of Machine Learning Research*, 17:1, 2016.

[44] K. Nokura. Paramagnetic unlearning in neural network models. *Physical Review E*, 54(5):5571, 1996.

[45] A.Y. Plakhov and S.A. Semenov. The modified unlearning procedure for enhancing storage capacity in Hopfield network. In *RNNS/IEEE Symposium on Neuroinformatics and Neurocomputers*, page 242, Rostov-on-Don, Russia, 1992.

[46] S. Wimbauer, N. Klemmer, and J.L. van Hemmen. Universality of unlearning. *Neural Networks*, 7(2):261, 1994.

[47] V.S. Dotsenko, N.D. Yarunin, and E.A. Dorotheev. Statistical mechanics of Hopfield-like neural networks with modified interactions. *Journal of Physics A: Mathematical and General*, 24(10):2419–2429, 1991.

[48] J.D. Creery, D.J. Brang, J.D. Arndt, A. Bassard, V.L. Towle, J.X. Tao, S. Wu, S. Rose, P.C. Warnke, N.P. Issa, and K.A. Paller. Electrophysiological markers of memory consolidation in the human brain when memories are reactivated during sleep. *Proceedings of the National Academy of Sciences*, 119(44):e2123430119, 2022.

[49] N. Maingret, G. Girardeau, R. Todorova, M. Goutierre, and M. Zugaro. Hippocampo-cortical coupling mediates memory consolidation during sleep. *Nature Neuroscience*, 19(7):959, 2016.

[50] G. Girardeau and V. Lopes-dos Santos. Brain neural patterns and the memory function of sleep. *Science*, 374(6567):560–564, 2021.

[51] G. Hinton. The Forward-Forward Algorithm: Some Preliminary Investigations. *arXiv:2212.13345*, 2022.

[52] J. Hinton and T.J. Sejnowski. *Unsupervised Learning: Foundations of Neural Computation*. The MIT Press, 1999.

[53] U.M. Tomasini, L. Petrini, F. Cagnetta, and M. Wyart. How deep convolutional neural networks lose spatial information with training. *arXiv:2210.01506*, 2023.

[54] L. Bonnasse-Gahot and J.P. Nadal. Categorical Perception: A Groundwork for Deep Learning. *Neural Computation*, 34(2):437, 2022.

[55] W.J. Johnston and S. Fusi. Abstract representations emerge naturally in neural networks trained to perform multiple tasks. *Nature Communications*, 14(1):1040, 2023.

[56] T. Kahnt and P.N. Tobler. Dopamine regulates stimulus generalization in the human hippocampus. *eLife*, 5:e12678, 2016. Publisher: eLife Sciences Publications, Ltd.

Appendix A: Reduction of the \mathcal{L} function

1. Training with noise

At each step of the algorithm a memory label μ_d is sampled at random and the update (11) is performed over the couplings. The new value of the \mathcal{L} function (17) is

$$\mathcal{L}' = -\frac{1}{\alpha N^2} \sum_{i,\mu}^{N,p} \operatorname{erf} \left(\frac{m\Delta_i^\mu}{\sqrt{2(1-m^2)}} + \frac{\lambda m}{N\sigma_i \sqrt{2N(1-m^2)}} \epsilon_i^{\mu_d} \xi_i^\mu \xi_i^{\mu_d} \sum_{j \neq i} S_j^{\mu_d} \xi_j^\mu \right). \quad (\text{A1})$$

Since $\delta\sigma_i \propto \frac{\lambda}{N} \frac{J_i}{\sigma_i} + O\left(\frac{\lambda}{N}\right)^3$ and the mean J_i of the couplings along line i equals zero by initialization and it is naturally maintained null during the algorithm, we have considered $\sigma'_i \simeq \sigma_i$. Then \mathcal{L}' can be rewritten as

$$\begin{aligned} \mathcal{L}' = & -\frac{1}{\alpha N^2} \sum_{i,\mu \neq \mu_d}^{N,p} \operatorname{erf} \left(\frac{m\Delta_i^\mu}{\sqrt{2(1-m^2)}} + O\left(\frac{1}{N}\right) \right) - \\ & - \frac{1}{\alpha N^2} \sum_i^N \operatorname{erf} \left(\frac{m\Delta_i^{\mu_d}}{\sqrt{2(1-m^2)}} + \frac{\lambda m \cdot m_t}{\sigma_i \sqrt{2N(1-m^2)}} \epsilon_i^{\mu_d} + O\left(\frac{1}{N}\right) \right), \end{aligned} \quad (\text{A2})$$

where we have used that $\frac{1}{N} \sum_{j \neq i} \xi_j^\mu S_j^{\mu_d} = O(N^{-1/2})$ when $\mu \neq \mu_d$ and $m_t = O(1)$. We thus expand the errorfunction at the first order in $O(N^{-1/2})$ obtaining the variations to \mathcal{L} in equation (19).

2. Training with structured noise

The new value of \mathcal{L} is derived by using equation (20) to evaluate the variation of stabilities

$$\begin{aligned} \mathcal{L}' = & -\frac{1}{\alpha N^2} \sum_{i,\mu}^{N,p} \operatorname{erf} \left(\frac{m\Delta_i^\mu}{\sqrt{2(1-m^2)}} + \frac{\lambda m \xi_i^\mu \xi_i^{\mu_d}}{2N\sigma_i \sqrt{2N(1-m^2)}} \sum_{j=1}^N S_j^{\mu_d} \xi_j^\mu + \frac{\lambda m \xi_i^\mu S_i^{\mu_d}}{2N\sigma_i \sqrt{2N(1-m^2)}} \sum_{j=1}^N \xi_j^{\mu_d} \xi_j^\mu - \right. \\ & \left. - \frac{\lambda m \xi_i^\mu S_i^{1,\mu_d}}{2N\sigma_i \sqrt{2N(1-m^2)}} \sum_{j=1}^N S_j^{\mu_d} \xi_j^\mu - \frac{\lambda m \xi_i^\mu S_i^{\mu_d}}{2N\sigma_i \sqrt{2N(1-m^2)}} \sum_{j=1}^N S_j^{1,\mu_d} \xi_j^\mu \right), \end{aligned} \quad (\text{A3})$$

where $\sigma'_i \simeq \sigma_i$ as in the previous paragraph. We now redefine $\chi_i^\mu = \xi_i^\mu S_i^{\mu_d}$, $\chi_i^{1,\mu} = \xi_i^\mu S_i^{1,\mu_d}$, $m_\mu = \frac{1}{N} \sum_{j=1}^N S_j^{\mu_d} \xi_j^\mu$ and $m_{1,\mu} = \frac{1}{N} \sum_{j=1}^N S_j^{1,\mu_d} \xi_j^\mu$ and expand the errorfunction at the first order in $O(N^{-1/2})$ obtaining

$$\delta\mathcal{L} = \frac{m\lambda}{\sqrt{2\pi\alpha^2 N^5 (1-m^2)}} \sum_{i,\mu}^{N,p} \frac{1}{2\sigma_i} \left[(m_\mu \chi_i^{1,\mu} + m_{1,\mu} \chi_i^\mu) - (m_\mu \xi_i^\mu \xi_i^{\mu_d} + M_\mu^{\mu_d} \chi_i^\mu) \right] \exp \left(-\frac{m^2 \Delta_i^{\mu^2}}{2(1-m^2)} \right) \quad (\text{A4})$$

where $M_\mu^{\mu_d} = \frac{1}{N} \sum_{i=1}^N \xi_i^\mu \xi_i^{\mu_d}$. Equation (A4) can be decomposed in

$$\delta\mathcal{L} = \delta\mathcal{L}_N + \delta\mathcal{L}_U \quad (\text{A5})$$

where $\delta\mathcal{L}_U$ contains the weight

$$\omega_i^\mu = \frac{1}{2\sigma_i} (m_\mu \chi_i^{1,\mu} + m_{1,\mu} \chi_i^\mu) \quad (\text{A6})$$

while $\delta\mathcal{L}_N$ contains

$$\Omega_i^\mu = \frac{1}{2\sigma_i} (m_\mu \xi_i^\mu \xi_i^{\mu_d} + M_\mu^{\mu_d} \chi_i^\mu) \quad (\text{A7})$$

We study the two contributions numerically, on a Hebbian network, i.e. with no learning going on, for the case of $m_t = 0^+$. The Pearson coefficient is measured between the vector of the stabilities Δ_i^μ and the weights ω_i^μ as well as

with Ω_i^μ separately. This quantity should underline an eventual reciprocal dependence between ω_i^μ , Ω_i^μ and Δ_i^μ . The test is repeated over states sampled by a Monte Carlo at different temperatures T . Results are reported in fig. 16a where it is evident that Ω_i^μ does not have any correlation with Δ_i^μ , while the dependence of ω_i^μ on the stabilities is evident. Moreover, we measured the indicator $\omega_{emp}(0)$, signaling the typical values of the weights ω_i^μ and Ω_i^μ when $\Delta_i^\mu \sim 0$ (see Section III A for further details), as reported in fig. 16b. The plot clearly shows that Ω_i^μ is small and generally fluctuating around zero. These aspects hold during the training procedure also, as it can be observed by performing the same measure at different step of the TWN procedure over states with $m_t = 0^+$. We will thus refer to $\delta\mathcal{L}_U$ as the relevant contribution to the variation of the function \mathcal{L} .

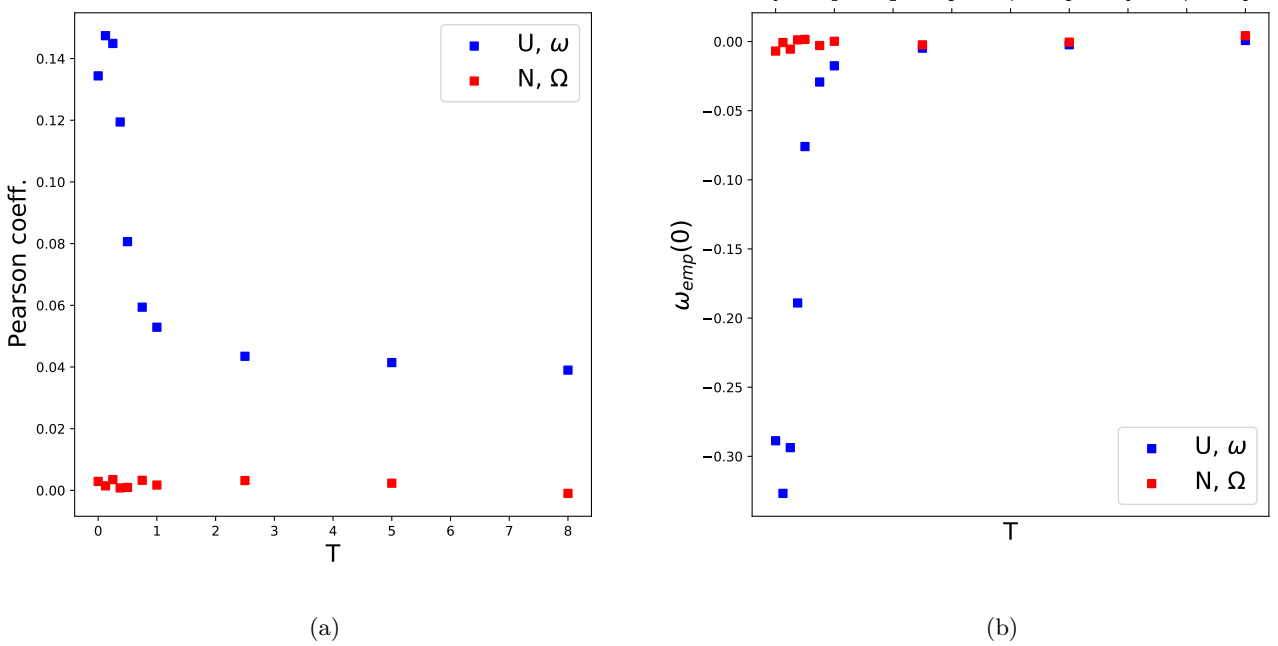


FIG. 16: (a) Pearson coefficient between ω_i^μ , Ω_i^μ and the stabilities Δ_i^μ , (b) $\omega_{emp}(0)$ for the case of a Hebbian network at different temperatures T . Configurations at a given temperature T have been sampled by a Monte Carlo of the Kawasaki kind, in order to choose only maximally noisy states ($m_t = 0^+$). Points are collected from 15 samples of the network. Choice of the parameters: $N = 500$, $\alpha = 0.5$.

Appendix B: Training with noise - computation of n_{SAT}

We now resume the computations performed in [30, 31] to explain how fig. 3 in the main text is made. We restrict ourselves to a spherical space of interactions such that

$$\sum_{j \neq i} J_{ij}^2 - N = 0 \quad \forall i \quad (B1)$$

We want to compute the probability distribution of the stabilities that now become

$$\Delta_i^\mu = \xi_i^\mu \sum_{j=1}^N \frac{J_{ij}}{\sqrt{N}} \xi_j^\mu \quad (B2)$$

The partition function of the model is then given by

$$Z = \int \prod_{i,j} dJ_{ij} \delta \left(\sum_{j \neq i} J_{ij}^2 - N \right) \exp \left(-\beta \mathcal{L}(m_t, J) \right) \quad (B3)$$

where β is the inverse annealing temperature of the problem and the loss function \mathcal{L} is defined in eq. (17). The distribution of the stabilities is

$$\rho_{m_t}(\Delta) = \overline{\frac{1}{Z} \int \prod_j dJ_{\bullet j} \delta \left(\sum_j J_{\bullet j}^2 - N \right) \exp \left(\beta \sum_{\mu} \operatorname{erf} \left(\frac{m_t \xi_{\bullet}^{\mu} \sum_j J_{\bullet j} \xi_j^{\mu}}{\sqrt{2N(1-m_t^2)}} \right) \right) \delta \left(\xi_{\bullet}^1 \sum_j \frac{J_{\bullet j}}{\sqrt{N}} \xi_j^1 - \Delta \right)}$$
 (B4)

Where $\overline{\cdot}$ denotes the average over the realizations of the memories and we have neglected the factorization over i , since we treat the optimization process as independent along the lines of the J_{ij} matrix. Index i has been nevertheless substituted by \bullet for the sake of completeness. Replicas can be used to evaluate the normalization, i.e.

$$1/Z = \lim_{n \rightarrow 0} Z^{n-1}$$
 (B5)

The replica calculation in the replica symmetric ansatz [2] when $\beta \rightarrow \infty$ leads to the following expression for $\rho_{m_t}(\Delta)$

$$\rho_{m_t}(\Delta) = \frac{1}{\sqrt{2\pi}} \left(1 + \sqrt{\frac{2}{\pi}} \frac{m_t^3 \chi}{(1-m_t^2)^{3/2}} \Delta \exp \left(-\frac{m_t^2 \Delta}{2(1-m_t^2)} \right) \right) \exp -\frac{w(\Delta)^2}{2}$$
 (B6)

where χ and w are derived by solving the following two equations

$$w = x - \frac{\sqrt{2}m_t \chi}{\sqrt{\pi(1-m_t^2)}} \exp \left(-\frac{m_t^2 x^2}{2(1-m_t^2)} \right)$$
 (B7)

$$\int_{-\infty}^{+\infty} Dw (x^*(w, \chi) - w)^2 = \alpha^{-1}$$
 (B8)

with x^* being the solution of (B7) and Dw being the standard Gaussian measure with zero mean and unitary variance. Eventually, the fraction of stable directions in the memories is computed as

$$n_{SAT}(m_t, \alpha) = \int_0^{+\infty} d\Delta \rho_{m_t}(\Delta)$$
 (B9)

Appendix C: Training with noise - measurement of the basins of attraction

We report here a general experimental procedure to measure the average size of the basins of attraction of a fully connected neural network of finite size N and a given choice of the control parameters.

The network is firstly trained according to an algorithm of our choice. Once the couplings have been found, the asynchronous version of dynamics (1) is initialized in one of the memories. The dynamics is run until convergence onto the attractor associated to the basin of belonging of the memory. Now the retrieval map $m_f(m_0)$ is measured with respect to that particular attractor and the procedure is repeated over different memories and realizations of the network. The average radius of the basin of attraction is then measured as the value of $1 - m_0$ where $m_f(m_0)$ equals a reference value. In our case such value is $m_f = 0.98$.

We have applied this procedure on networks trained either as SVMs and with the TWN algorithm. In the former case a convex algorithm contained in the *cvxpy* Python domain [43] is implemented to train the network. To be more specific, N independent machines are trained to correctly classify $p = \alpha N$ binary memories of the kind of $\vec{\xi}^{\mu} \in \{-1, +1\}^N$ having as labels ξ_i^{μ} with $i \in [1, \dots, N]$.

Regarding the dynamics, the stability of fixed points is in general implied by some properties of the couplings, mainly their degree of symmetry. For the case of the TWN algorithm we start from a random symmetric matrix, as done in [11]: the update of the couplings will only perturb the initial symmetry yet allowing the measures to be still consistent with the theory. On the other hand, numerics show that SVMs are sufficiently symmetric to let the asynchronous dynamics converge. The comparison between the retrieval maps obtained for the two algorithms with $\alpha = 0.45$ and $N = 200$ is reported in fig. 17. The curve relative to the SVM is fixed, while the one associated with the TWN is changing with respect to the training overlap m_t .

Even if the SVM always reaches classification of the memories for $\alpha < 2$ [9], a network trained with noise might show two different behaviors: one associated to *retrieval* where each memory is close to an attractor, and one related to *non-retrieval* where the memory is far from its attractor and the basins of attraction might contain orthogonal configurations with respect to the central attractor. In particular network models where couplings are assembled according to particular rules (e.g. [12], [47]) the transition between these two regimes can be computed analytically.

In the case of TWN this cannot be done. It is then important to find an empirical criterion to divide the two behaviors as a function of (α, m_t) .

Let us assume that when $N \gg 1$ the retrieval map $m_f(m_0)$ develops a plateau starting from $m_0 = 1$ and ending in some limit value $m_0 = m_c < 1$ such that $m_f = 1$ along all this interval. Hence one can associate the formation of such a plateau with the existence of a cohesive basin of attraction, where close configurations in hamming distance to the attractor converge to the attractor. One then wants to measure the value of m_t at which such property of the basin disappears. As a possible estimate, it is convenient to consider the m_t^* such that

$$\frac{dm_f}{dm_0}(m_t^*) \Big|_{m_0=1} = 1. \quad (\text{C1})$$

The numerical extrapolation of the overlap in fig. 4 at different values of N shows a good agreement between the approximate separation between the two regions showed in fig. 4 and the line estimated by condition (C1).

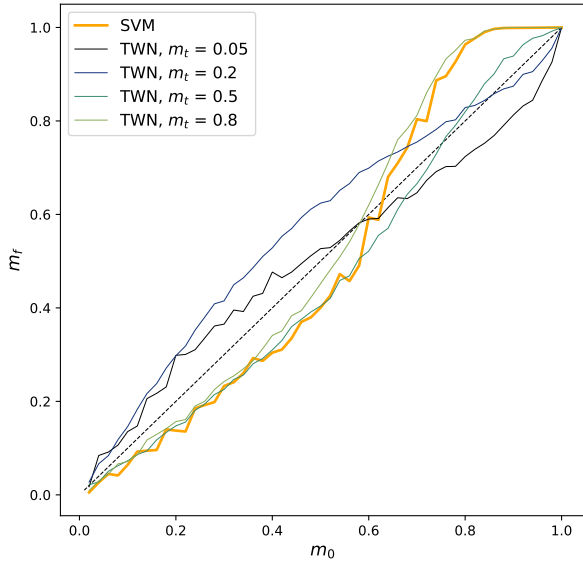


FIG. 17: Retrieval map $m_f(m_0)$ in the case of networks trained through SVM and TWN algorithms. Curves are shown as a function of m_t and compared with the bisector, indicated with a *dashed black* line. Points are averaged over 10 samples. Choice of the parameters: $N = 200$, $\alpha = 0.45$.